Calculation of space-charge tune shift in a cylindrical chamber for bunched beams employing Green's function formalism

Yoshihiro Shobuda

JAEA, Japan Atomic Energy Agency, 2-4 Shirakata, Tokaimura, Nakagun, Ibaraki 319-1195, Japan

When computing the space-charge tune shift for a relativistic bunched beam within a cylindrical chamber, mirror currents for a coasting beam, initially introduced to replace the chamber wall, are employed. Subsequently, the obtained result is extended to encompass the bunched beam, taking into account the bunching factor which quantifies the distribution of bunches around the accelerator ring. In the process of derivation, the terms that characterize the bunch length are intuitively integrated into the formula. As a result, the validity of this approach has never been established. This study provides the derivation of the space-charge tune shift formula for both relativistic and nonrelativistic bunched beams right from the outset, employing the Green function formalism. Subsequently, it is compared with the earlier formula derived using mirror currents.

I. INTRODUCTION

When generating high-intensity beams in contemporary accelerators [1,2], it becomes essential to assess both the coherent and incoherent space-charge tune shifts [3–8]. Understanding the impact of the chamber boundary on the tune shifts holds particular significance, as it enables the evaluation of space-charge damping effects on beam instabilities [9,10].

The significance of acknowledging the space-charge tune shift resulting from the presence of the chamber boundary was initially identified and articulated by Laslett [11]. Presently, his research findings have been cited in numerous accelerator textbooks and reports [3–8].

The formulas for the coherent ($\Delta\nu_{sp,coh}$) and incoherent space-charge tune shifts ($\Delta\nu_{sp,incoh}$) of a Gaussian beam, with identical standard deviations in both horizontal and vertical directions, within a cylindrical chamber of radius a, can be expressed as follows:

for the coherent space-charge tune shift:

$$\Delta\nu_{sp,coh} = -\frac{r_p N_p R}{2\pi\nu_{T,0} B \beta_s^2 \gamma_s^3} \left[\frac{2(1+\beta_s^2\gamma_s^2 B)}{a^2}\left(\frac{1}{2}\right) + \frac{2\beta_s^2\gamma_s^2 B}{g^2}\left(\frac{\pi^2}{16}\right)\eta_b \right], \quad (1)$$

for the incoherent space-charge tune shift:

$$\Delta\nu_{sp,incoh} = -\frac{r_p N_p R}{2\pi\nu_{T,0} B \beta_s^2 \gamma_s^3} \left[\frac{1}{2\sigma_x^2} + \frac{2\beta_s^2\gamma_s^2 B}{g^2}\left(\frac{\pi^2}{24}\right)\eta_b \right]. \quad (2)$$

These formulas (1) and (2) consider both the conductive chamber with radius a and the ferromagnetic boundaries with radius g. Here, β_s and γ_s denote Lorentz-β_s and -γ_s, r_p represents the classical particle radius, N_p signifies the total number of particles in the accelerator ring, $\nu_{T,0}$ stands for one of the unperturbed tunes on the transverse plane, $2\pi R$ denotes the circumference of the ring, and B corresponds to the bunching factor, which quantifies the bunch occupation around the ring, defined by the equation:

$$B = \frac{n_b \sqrt{2\pi}\sigma_z}{2\pi R}, \quad (3)$$

where n_b indicates the number of bunches, and σ_z denotes the standard deviation of the bunch length, assuming a Gaussian distribution for the beam. The magnetic filling factor η_b is defined as $\eta_b = L_{\text{mag}}/2\pi R$, where L_{mag} represents the combined length of magnets with radius g around the ring circumference.

Regarding the incoherent tune shifts, it is important to note that the contribution solely originates from the direct space-charge effect, without any involvement of the indirect space-charge force in the case of $\eta_b = 0$.

A renowned and foundational text, exemplified by the citation [4], outlines the direct space-charge's potential impact on the coherent tune shift through equations (10.44) and (10.48), as well as equations (21.67) and (21.71) in its revised edition [5], incorporating the direct space-charge

contribution. This discrepancy becomes notable, given that the initial work by Laslett [11] omits such a term. Consequently, within this paper, we explicitly address the accuracy of this description.

Meanwhile, it is important to emphasize that the formula (1) is applicable exclusively to a thin vacuum chamber where the ac magnetic fields can penetrate the walls, much like the dc component, as discussed in Refs. [7,12]. As a more typical case, Zötter studied scenarios in which a relativistic beam passes through a thick chamber, where the skin depth is smaller than the square root of the product of the chamber's radius and thickness, and modified the formula [7,12].

Reference [8] summarizes the formulas of the tune shifts in the thick chamber in different boundary geometries, including parallel plates, cylindrical, and elliptical chambers. The horizontal coherent and incoherent tune shift can be simplified as

$$\Delta \nu_{sp,coh} = -\frac{r_p N_p \langle \beta_x \rangle}{2\pi a^2 B_f \beta_s^2 \gamma_s^3}, \tag{4}$$

and

$$\Delta \nu_{sp,incoh} = -\frac{r_p N_p \langle \beta_x \rangle}{2\pi B_f \beta_s^2 \gamma_s^3} \frac{1}{2\sigma_x^2}, \tag{5}$$

for a uniform cylindrical conductive chamber in an accelerator with an average of horizontal β function: $\langle \beta_x \rangle$, which is sometimes approximated as

$$\langle \beta_x \rangle = \frac{R}{\nu_{T,0}}, \tag{6}$$

with the average radius of the ring R and the unperturbed tune $\nu_{T,0}$. In the above formulas, the bunching factor B_f is defined as

$$B_f = \frac{n_b l}{S 2\pi R}. \tag{7}$$

The definition of B_f is contingent on the particular bunch shape, with l denoting the overall bunch length and S representing a numerical factor that adapts to the given bunch shape. When dealing with Gaussian bunches, the values assigned to l and S are $4\sigma_z$ and 1.6, respectively. In practical terms, the numerical value of B_f for a Gaussian beam is nearly indistinguishable from that found in Eq. (3).

It is worth noting that the Lorentz-β and-γ dependence in Eq. (4) differs significantly from that in Eq. (1). This distinction is attributed to the factor $(1 + \beta_s^2 \gamma_s^2 B)$ in Eq. (1), especially when $\eta_b = 0$. On the other hand, Eqs. (2) and (5) exhibit almost identical behavior under the condition.

However, during the derivation of the aforementioned formulas, a substitution of the boundary condition is introduced, specifically involving mirror currents for coasting beams. This substitution is necessitated by the inherent challenges in integrating boundary effects into calculations related to the impact of space charge on bunched beams. As a result, the expressions for bunched beams are developed by extending the formulations initially devised for coasting beams, a process facilitated by the introduction of the bunching factor. Therefore, a more advanced formalism is essential to validate the approach relying on image currents.

Our investigation revolves around verifying whether the derived formulas exhibit the Lorentz-γ dependence, as proposed by the mirror currents approach, when a Gaussian bunched beam travels through a cylindrical chamber characterized by conductivity and permeability. Furthermore, we investigate the potential influence of the chamber's conductivity or permeability on the magnitude of the tune shifts when the wakefield effects generated by previous bunches are disregarded [13].

This study is dedicated to systematically deriving space-charge tune shifts for a bunched beam within a thick chamber, utilizing the Green function approach under the assumption of translational symmetry, resulting in setting η_b to zero. Consequently, the derived formulas are suitable for comparison with formulas (4) and (5).

The paper is organized as follows: In Sec. II, we introduce previous expressions [14,15] for tune shifts of a bunched beam without any boundaries, using the familiar Green function technique and devoid of boundary conditions. Meanwhile, we review the formalism for incorporating the boundary effect into the tune shifts based on the mirror currents of a coasting beam. Subsequently, in Sec. III, we address the coherent and incoherent tune shifts for a bunched beam within a cylindrical chamber in a more integrated manner. This is achieved by employing the Green function approach, incorporating cylindrical boundary conditions, and considering both conductivity and permeability effects. In this section, we also validate the results against earlier formulations. Finally, Sec. IV concludes this paper.

II. CONVENTIONAL APPROACH FOR CALCULATING SPACE-CHARGE TUNE SHIFTS

A. Tune shift due to space-charge effects in a Gaussian beam without considering any boundaries

This section calculates the direct space-charge effects on a bunched Gaussian beam based on the Green function formalism. The Poisson equation in the reference frame of a beam moving along the z axis is expressed as follows:

$$\frac{\partial^2 \bar{\Phi}}{\partial x^2} + \frac{\partial^2 \bar{\Phi}}{\partial y^2} + \frac{\partial^2 \bar{\Phi}}{\partial \bar{z}^2} = -\frac{cZ_0 e N_b}{(2\pi)^{3/2} \sigma_x \sigma_y \bar{\sigma}_z} e^{-\frac{x^2}{2\sigma_x^2} - \frac{y^2}{2\sigma_y^2} - \frac{\bar{z}^2}{2\bar{\sigma}_z^2}}, \tag{8}$$

where

$$\bar{\sigma}_z = \gamma_s \sigma_z. \tag{9}$$

Here, $\bar{\Phi}(x, y, \bar{z})$ represents the scalar potential in the rest frame $(c\bar{t}, x, y, \bar{z})$, e signifies the elementary electric

charge, c stands for the speed of light, $Z_0 = 120\pi \ \Omega$ denotes the impedance of free space, σ_x and σ_y represent the horizontal and vertical standard deviations, respectively, and N_b represents the number of particles per bunch. Reference [14] provides the expression of the scalar potential $\bar{\Phi}(x, y, \bar{z})$ as

$$\bar{\Phi}(x,y,\bar{z}) = \frac{eN_b c Z_0}{2(2\pi)^{3/2}} \int_0^\infty \frac{e^{-\frac{1}{2}\left(\frac{x^2}{\sigma_x^2+\xi_0}+\frac{y^2}{\sigma_y^2+\xi_0}+\frac{\bar{z}^2}{\bar{\sigma}_z^2+\xi_0}\right)}}{\sqrt{(\sigma_x^2+\xi_0)(\sigma_y^2+\xi_0)(\bar{\sigma}_z^2+\xi_0)}} d\xi_0, \quad (10)$$

whose concrete derivation is explained in Appendix A. Without loss of generality, we can introduce the transverse position of the source particle (x_0, y_0) replacing Eq. (10) as

$$\bar{\Phi}(x, y, \bar{z}; x_0, y_0)$$
$$= \frac{eN_b c Z_0}{2(2\pi)^{3/2}} \int_0^\infty \frac{e^{-\frac{1}{2}\left(\frac{(x-x_0)^2}{\sigma_x^2+\xi_0}+\frac{(y-y_0)^2}{\sigma_y^2+\xi_0}+\frac{\bar{z}^2}{\bar{\sigma}_z^2+\xi_0}\right)}}{\sqrt{(\sigma_x^2+\xi_0)(\sigma_y^2+\xi_0)(\bar{\sigma}_z^2+\xi_0)}} d\xi_0, \quad (11)$$

which can be expanded for small (x, y) and (x_0, y_0).

The scalar potential Φ and vector potential A_z in the laboratory frame (ct, x, y, z) undergo transformations as follows:

$$\Phi(x, y, z - \beta_s ct) = \gamma_s \bar{\Phi}[x, y, \gamma_s(z - \beta_s ct)], \quad (12)$$

$$A_z(x, y, z - \beta_s ct) = \frac{\beta_s}{c} \gamma_s \bar{\Phi}[x, y, \gamma_s(z - \beta_s ct)]. \quad (13)$$

In these equations, the relationship between the coordinates in the rest frame and the laboratory frame is governed by the equations:

$$c\bar{t} = \gamma_s(ct - \beta_s z), \quad (14)$$

$$\bar{z} = \gamma_s(z - \beta_s ct). \quad (15)$$

Space charge is occasionally formulated in terms of the scalar potential $\bar{\Phi}(x, y, \bar{z})$ in the rest frame because certain simulation programs that handle space-charge effects calculate them in the rest frame of the beam, then transform them in the laboratory frame [16].

When the electromagnetic fields are expanded around small values of (x, y), and (x_0, y_0), the horizontal space-charge tune shift can be expressed as [4,5,17]:

$$\Delta\nu_{sp,coh}$$
$$= \frac{2\pi R\langle\beta_x\rangle}{4\pi}\left[\frac{\partial^2}{\partial x^2}\frac{e\Phi(x,y,z-\beta_s ct;x_0,y_0)}{m_p c^2\beta_s^2\gamma_s^3}\right.$$
$$\left.+\frac{\partial^2}{\partial x\partial x_0}\frac{e\Phi(x,y,z-\beta_s ct;x_0,y_0)}{m_p c^2\beta_s^2\gamma_s^3}\right]\Bigg|_{x=y=x_0=y_0=0,z=\beta_s ct},$$
$$(16)$$

for coherent tune shift and

$$\Delta\nu_{sp,incoh}$$
$$= \frac{2\pi R\langle\beta_x\rangle}{4\pi}\frac{\partial^2}{\partial x^2}\frac{e\Phi(x,y,z-\beta_s ct;x_0,y_0)}{m_p c^2\beta_s^2\gamma_s^3}\Bigg|_{x=y=x_0=y_0=0}, \quad (17)$$

for incoherent tune shift, or equivalently:

$$\Delta\nu_{sp,coh}$$
$$= \frac{2\pi R\langle\beta_x\rangle}{4\pi}\left[\frac{\partial^2}{\partial x^2}\frac{e\bar{\Phi}(x,y,\gamma_s(z-\beta_s ct);x_0,y_0)}{m_p c^2\beta_s^2\gamma_s^2}\right.$$
$$\left.+\frac{\partial^2}{\partial x\partial x_0}\frac{e\bar{\Phi}(x,y,\gamma_s(z-\beta_s ct);x_0,y_0)}{m_p c^2\beta_s^2\gamma_s^2}\right]\Bigg|_{x=y=x_0=y_0=0,z=\beta_s ct},$$
$$(18)$$

$$\Delta\nu_{sp,incoh}$$
$$= \frac{2\pi R\langle\beta_x\rangle}{4\pi}\frac{\partial^2}{\partial x^2}\frac{e\bar{\Phi}(x,y,\gamma_s(z-\beta_s ct);x_0,y_0)}{m_p c^2\beta_s^2\gamma_s^2}\Bigg|_{x=y=x_0=y_0=0}, \quad (19)$$

where m_p represents the mass of the particle because the coherent tune shift for an axisymmetric Gaussian beam is computed via fields at the observed point (x, y, z), identifying with the bunch centroid $(x_0, y_0, \beta_s ct)$.

In the process of calculating the vertical tune shift, the horizontal β function and the derivative found in Eqs. (16)–(19) with respect to the horizontal coordinates x or x_0 are substituted with the vertical β function and the derivative associated with the vertical coordinates y or y_0.

The coherent tune shift for the Gaussian beam is concretely, calculated with Eq. (11) as follows:

$$\frac{\partial^2\bar{\Phi}(x,y,\bar{z};x_0,y_0)}{\partial x^2} + \frac{\partial^2\bar{\Phi}(x,y,\bar{z};x_0,y_0)}{\partial x_0\partial x} = 0, \quad (20)$$

demonstrating the coherent tune shift is identical to zero due to the absence of boundary conditions, which is consistent with Eqs. (1) and (4). This lack of contribution from direct space charge to the coherent tune shift is indicative of the inherent symmetry of space.

When dealing with the incoherent tune shift of an axisymmetric Gaussian beam, we make use of Eq. (10) with $\sigma_x = \sigma_y$ and make an approximation for small values of x and y:

$$\bar{\Phi}(x,y,\bar{z}) = \frac{eN_b c Z_0}{2(2\pi)^{3/2}} \int_0^\infty \frac{e^{-\frac{\bar{z}^2}{2(\bar{\sigma}_z^2+\xi_0)}}}{\sqrt{(\sigma_x^2+\xi_0)^2(\bar{\sigma}_z^2+\xi_0)}} d\xi_0$$
$$+ \bar{\Phi}^{(II)}(x,y,\bar{z}), \quad (21)$$

where the second term $\bar{\Phi}^{(II)}$ is contingent upon the transverse coordinates (x, y):

$$\bar{\Phi}^{(II)}(x,y,\bar{z}) = -\frac{eN_b cZ_0(x^2+y^2)}{4(2\pi)^{3/2}}$$

$$\times \int_0^\infty \frac{e^{-\frac{\bar{z}^2}{2(\bar{\sigma}_z^2+\xi_0)}}}{(\sigma_x^2+\xi_0)^2\sqrt{(\bar{\sigma}_z^2+\xi_0)}}d\xi_0, \quad (22)$$

and is further approximated for large $\bar{\sigma}_z$ as

$$\bar{\Phi}^{(II)}(x,y,\bar{z}) \simeq -\frac{eN_b cZ_0(x^2+y^2)}{8\sqrt{2}\pi^{\frac{3}{2}}\sigma_x^2\bar{\sigma}_z}. \quad (23)$$

Substituting Eq. (23) into Eq. (18), we rederive the first term (direct space-charge tune shift) in Eqs. (2) and (5) as

$$\Delta\nu_{sp,incoh} = -\frac{r_p N_p R}{2\pi\nu_{T,0}B\beta_s^2\gamma_s^3}\frac{1}{2\sigma_x^2}. \quad (24)$$

In this derivation, we utilize the approximate relationship of Eq. (6), define $N_p = n_b N_b$, and use the definition of the bunching factor as given by Eq. (3).

Let us investigate whether the approach with a coasting beam can yield the same formula. The scalar potential in the laboratory frame, denoted as $\Phi(x,y,z-\beta_s ct)$, is expressed as

$$\Phi(x,y,z-\beta_s ct)$$
$$= \gamma_s \frac{eN_b cZ_0}{2(2\pi)^{3/2}}\int_0^\infty \frac{e^{-\frac{1}{2}\left(\frac{x^2}{\sigma_x^2+\xi_0}+\frac{y^2}{\sigma_y^2+\xi_0}+\frac{\gamma_s^2(z-\beta_s ct)^2}{\gamma_s^2\sigma_z^2+\xi_0}\right)}}{\sqrt{(\sigma_x^2+\xi_0)(\sigma_y^2+\xi_0)(\gamma_s^2\sigma_z^2+\xi_0)}}d\xi_0,$$
$$(25)$$

which pertains to the three-dimensional scenario through transformation relations provided by Eq. (12) with Eqs. (9) and (10).

Now, if we modify Eq. (25) by replacing $\bar{z}$ with $\bar{z}-z_i$ before integrating the scalar potential over z_i from negative infinity to positive infinity, while also dividing it by the circumference $2\pi R$, we arrive at the two-dimensional scalar potential $\Phi_{2D}(x,y)$:

$$\Phi_{2D}(x,y) = \frac{\tilde{\lambda}cZ_0}{4\pi}\int_0^\infty \frac{e^{-\frac{1}{2}\left(\frac{x^2}{\sigma_x^2+\xi_0}+\frac{y^2}{\sigma_y^2+\xi_0}\right)}}{\sqrt{(\sigma_x^2+\xi_0)(\sigma_y^2+\xi_0)}}d\xi_0, \quad (26)$$

which holds for a longitudinally uniform beam given by

$$\rho_{2D} = \frac{\tilde{\lambda}}{2\pi\sigma_x\sigma_y}e^{-\frac{x^2}{2\sigma_x^2}-\frac{y^2}{2\sigma_y^2}}, \quad (27)$$

thus reproducing the scalar potential formula presented in Ref. [15]. Here, $\tilde{\lambda}$ represents the line density.

Since Eq. (26) with $\sigma_x = \sigma_y$ is approximated as

$$\Phi_{2D}(x,y) \simeq \frac{\tilde{\lambda}cZ_0}{4\pi}\int_0^\infty \frac{d\xi_0}{(\sigma_x^2+\xi_0)} - \frac{\tilde{\lambda}cZ_0}{8\pi\sigma_x^2}(x^2+y^2), \quad (28)$$

when considering small values of x and y, we can reproduce formula (24) for the incoherent tune shift, which comes from substituting Eq. (28) into Eq. (17), while also utilizing the definition of the bunching factor as presented in Eq. (3).

Emphasizing the crucial role played by the assumption concerning the line density,

$$\tilde{\lambda} = \frac{eN_p}{n_b\sqrt{2\pi}\sigma_z}, \quad (29)$$

is of paramount importance within this derivation. This becomes particularly evident when delving into the derivation process for the two-dimensional potential $\Phi_{2D}(x,y)$. In this process, the initial step involves substituting $\bar{z}$ with $\bar{z}-z_i$ in the expression for the three-dimensional potential, as outlined in Eq. (25). Subsequently, integration over z_i spans the entirety of the range from negative infinity to positive infinity. However, it is noteworthy that due to the nuanced nature of the mathematical procedure involved, it is not a perfect match to the aforementioned assumption. Therefore, the intricate interplay between this assumption and the sequence of mathematical steps remains pivotal for the successful completion of the derivation.

B. Evaluating the effects of chamber boundary with mirror currents

Following Ref. [7], let us solve the Poisson equation in the laboratory frame:

$$\Delta\Phi(x,y,z-\beta_s ct) = -cZ_0\tilde{\lambda}\delta(x-x_0)\delta(y-y_0), \quad (30)$$

for a coasting beam within a cylindrical chamber with radius a. The solution, which satisfies $\Phi(x,y,z-\beta_s ct) = \log[(x_0^2+y_0^2)/a^2]$ being constant on the chamber boundary with $\rho = a$, is expressed as

$$\Phi(x,y,z-\beta_s ct) = \Phi_s(x,y,z-\beta_s ct) + \Phi_{\text{Im}}(x,y,z-\beta_s ct), \quad (31)$$

where the scalar potential $\Phi_s(x,y,z-\beta_s ct)$ created by the source particle and $\Phi_{\text{Im}}(x,y,z-\beta_s ct)$ due to the boundary are, respectively, described as

$$\Phi_s(x,y,z-\beta_s ct) = \frac{cZ_0\tilde{\lambda}}{4\pi}\log[(x-x_0)^2+(y-y_0)^2], \quad (32)$$

$$\Phi_{\mathrm{Im}}(x, y, z - \beta_s ct) = -\frac{cZ_0\tilde{\lambda}}{4\pi} \log\left[\left(x - \frac{a^2 x_0}{(x_0^2 + y_0^2)}\right)^2\right.$$

$$\left. + \left(y - \frac{a^2 y_0}{(x_0^2 + y_0^2)}\right)^2\right], \quad (33)$$

producing

$$\frac{\partial \Phi_s(x, y, z - \beta_s ct)}{\partial x} = \frac{cZ_0\tilde{\lambda}}{2\pi} \frac{(x - x_0)}{[(x - x_0)^2 + (y - y_0)^2]}, \quad (34)$$

$$\frac{\partial \Phi_{\mathrm{Im}}(x, y, z - \beta_s ct)}{\partial x}$$

$$= -\frac{cZ_0\tilde{\lambda}}{2\pi} \frac{\left(x - \frac{a^2 x_0}{(x_0^2 + y_0^2)}\right)}{\left[\left(x - \frac{a^2 x_0}{(x_0^2 + y_0^2)}\right)^2 + \left(y - \frac{a^2 y_0}{(x_0^2 + y_0^2)}\right)^2\right]}. \quad (35)$$

In this context, the scalar potential $\Phi_{\mathrm{Im}}(x, y, z - \beta_s ct)$ is analogous to the potential generated by the mirror current positioned at $[a^2 x_0/(x_0^2 + y_0^2), a^2 y_0/(x_0^2 + y_0^2)]$, effectively substituting the chamber boundary.

The computation of the contributions to the coherent $\Delta\nu_{sp,coh}^{\mathrm{Im}}$ and incoherent $\Delta\nu_{sp,incoh}^{\mathrm{Im}}$ tune shifts arising from the mirror current is performed as follows:

$$\Delta\nu_{sp,coh}^{\mathrm{Im}}$$

$$= \frac{2\pi R\langle\beta_x\rangle}{4\pi}\left[\frac{\partial^2}{\partial x^2}\frac{e\Phi_{\mathrm{Im}}(x, y, z - \beta_s ct; x_0, y_0)}{m_p c^2 \beta_s^2 \gamma_s^3}\right.$$

$$\left. + \frac{\partial^2}{\partial x \partial x_0}\frac{e\Phi_{\mathrm{Im}}(x, y, z - \beta_s ct; x_0, y_0)}{m_p c^2 \beta_s^2 \gamma_s^3}\right]\Bigg|_{x=y=x_0=y_0=0, z=\beta_s ct}$$

$$= \frac{r_p N_p\langle\beta_x\rangle}{2\pi a^2 (\frac{n_b\sqrt{2\pi}\sigma_z}{2\pi R})\beta_s^2 \gamma_s^3}, \quad (36)$$

$$\Delta\nu_{sp,incoh}^{\mathrm{Im}}$$

$$= \frac{2\pi R\langle\beta_x\rangle}{4\pi} \frac{\partial^2}{\partial x^2}\frac{e\Phi_{\mathrm{Im}}(x, y, z - \beta_s ct; x_0, y_0)}{m_p c^2 \beta_s^2 \gamma_s^3}\Bigg|_{x=y=x_0=y_0=0} = 0. \quad (37)$$

These expressions are derived using Eqs. (16) and (17), under the assumption stated in Eq. (29). Although Eq. (34) is not Taylor expanded for small values of (x, y) and (x_0, y_0), the symmetry ensures that

$$\frac{\partial^2 \Phi_s(x, y, z - \beta_s ct; x_0, y_0)}{\partial x^2}$$

$$+ \frac{\partial^2 \Phi_s(x, y, z - \beta_s ct; x_0, y_0)}{\partial x \partial x_0} = 0, \quad (38)$$

demonstrating no contribution of the direct space-charge effect to the coherent tune shift. On the other hand,

$$\frac{\partial^2 \Phi_s(x, y, z - \beta_s ct)}{\partial x^2}\Bigg|_{x=x_0=y=y_0=0}, \quad (39)$$

becomes infinite due to the self-energy of the point particle, consistent with formula (5). Thus, formulas (4) and (5) can be reproduced by combining Eqs. (20), (24), (36), and (37) in a conventional manner.

In the next section, the coherent and incoherent tune shifts for a bunched beam within a cylindrical chamber are addressed more integratively by employing the Green's function approach with cylindrical boundary conditions.

III. A SOLUTION TO A POISSON EQUATION WITHIN A CYLINDRICAL CHAMBER

In this section, we will illustrate the approach to solving the Poisson equation for an axisymmetric Gaussian bunched beam within a conductive cylindrical chamber of radius a. The Poisson equation in the rest frame of the beam $(c\bar{t}, x, y, \bar{z})$ can be expressed as

$$\frac{\partial^2 \bar{\Phi}}{\partial x^2} + \frac{\partial^2 \bar{\Phi}}{\partial y^2} + \frac{\partial^2 \bar{\Phi}}{\partial \bar{z}^2} = -cZ_0\bar{\rho}_p(x, y, \bar{z}), \quad (40)$$

where $\bar{\rho}_p(x, y, \bar{z})$ is defined by

$$\bar{\rho}_p(x, y, \bar{z}) = eN_b\hat{\rho}(\bar{z})\frac{e^{\frac{(\rho\cos\varphi - r_0\cos\theta_0)^2 + (\rho\sin\varphi - r_0\sin\theta_0)^2}{2\sigma_x^2}}}{2\pi\sigma_x^2}, \quad (41)$$

and $\hat{\rho}(\bar{z})$ is given by

$$\hat{\rho}(\bar{z}) = \frac{e^{-\frac{\bar{z}^2}{2\bar{\sigma}_z^2}}}{\sqrt{2\pi}\bar{\sigma}_z} = \int_{-\infty}^{\infty}\frac{d\bar{k}}{2\pi}e^{-\mathbf{j}\bar{k}\bar{z}}e^{-\frac{1}{2}\bar{k}^2\bar{\sigma}_z^2}, \quad (42)$$

where $\mathbf{j}$ is the imaginary unit. Additionally, we introduce the polar coordinates $(\rho, \varphi, \bar{z})$ as

$$x = \rho\cos\varphi, \quad (43)$$

$$y = \rho\sin\varphi, \quad (44)$$

and the center of the bunch on the horizontal plane is given by $(r_0\cos\theta_0, r_0\sin\theta_0)$.

Let us begin by considering the boundary condition (I) within the context of a conductive chamber characterized by a conductivity of σ. The thickness of this chamber is assumed to exceed the skin depth, denoted as $\delta = \sqrt{2/(\omega\mu_0\sigma)} = \sqrt{2/(k\beta_s Z_0\sigma)}$, where ω represents the angular frequency and μ_0 stands for the vacuum's magnetic permeability.

In this scenario, we can deduce an approximate relationship for the electromagnetic fields that are proportionate to $e^{\mathbf{j}\omega t - \mathbf{j}kz}$ at the boundary defined by $\rho = a$ as follows:

$$E_z \simeq -\frac{(1+\mathbf{j})}{2}\frac{\omega}{c}Z_0\sqrt{\frac{2}{\omega\mu_0\sigma}}H_\varphi. \tag{45}$$

This outcome arises after solving Maxwell's equations:

$$\mathrm{rot}E = -\mathbf{j}\omega\mu_0 H, \tag{46}$$

$$\mathrm{rot}H = \sigma E, \tag{47}$$

within the context of a chamber with infinite thickness, as discussed within the laboratory frame (as referenced in [13,18]).

We can convert Eq. (45) into its rest-frame equivalent, resulting in

$$\bar{E}_z \simeq \frac{(1+\mathbf{j})}{2}\gamma_s\beta_s\bar{k}\sqrt{\frac{2}{\gamma_s\beta_s\bar{k}Z_0\sigma}}\gamma_s\beta_s\bar{E}_\rho. \tag{48}$$

This corresponds to the expression:

$$\bar{\Phi}(x,y,\bar{z}) \simeq \sqrt{\frac{\gamma_s^3\beta_s^3}{\mathbf{j}\bar{k}Z_0\sigma}}\frac{\partial\bar{\Phi}(x,y,\bar{z})}{\partial\rho}, \tag{49}$$

where $\bar{\Phi}(x,y,\bar{z})$ represents the scalar potential in the rest frame. The quantities $\bar{\omega}$ and $\bar{k}$, which relate to the angular frequency and wavelength in the rest frame, respectively, are linked to their counterparts ω and k in the laboratory frame as follows:

$$\frac{\bar{\omega}}{c} = \gamma_s\left(\frac{\omega}{c} - \beta_s k\right) = 0, \tag{50}$$

and

$$\bar{k} = \gamma_s\left(k - \beta_s\frac{\omega}{c}\right) = \frac{k}{\gamma_s}. \tag{51}$$

Furthermore, when we consider the boundary condition (II) imposed by a conductive ferromagnetic chamber with relative permeability μ' and conductivity σ, the relation in Eq. (45) between the fields in the laboratory frame takes on a more general form:

$$E_z \simeq -\frac{\omega}{c}\mu'Z_0\sqrt{\frac{\mathbf{j}}{\omega\mu'\mu_0\sigma}}H_\varphi. \tag{52}$$

This results in a corresponding relation for the scalar potential in the rest frame:

$$\bar{\Phi}(x,y,\bar{z}) = \sqrt{\frac{\beta_s^3\gamma_s^3\mu'}{\mathbf{j}\bar{k}Z_0\sigma}}\frac{\partial\bar{\Phi}(x,y,\bar{z})}{\partial\rho}, \tag{53}$$

replacing the earlier Eq. (49). In essence, Eq. (53) can be seen as a generalized boundary condition, accommodating both conductive and magnetic boundary walls.

The interplay between this boundary condition and the Poisson equation constitutes the foundational aspects of the problem that we will delve into more extensively.

The Green's function $G(\vec{r},\vec{r}')$, which fulfills the boundary condition stated in Eq. (53) at $\rho = a$, is provided as [19]:

$$G(\vec{r},\vec{r}') = \sum_{m=0}^{\infty}\frac{\epsilon_m}{2\pi^2}\cos m(\varphi - \varphi')$$

$$\times \int_0^\infty d\lambda\mathcal{F}_m(\rho;\rho')\cos[\lambda(\bar{z} - \bar{z}')]. \tag{54}$$

Here, the function $\mathcal{F}_m(\rho;\rho')$ takes the form:

$$\mathcal{F}_m(\rho;\rho') = \begin{cases} \left[K_m(\lambda\rho') - \dfrac{\left(-\sqrt{\frac{\beta_s^3\gamma_s^3\mu'}{\mathbf{j}\bar{k}Z_0\sigma}}\lambda K'_m(\lambda a)+K_m(\lambda a)\right)}{\left(-\sqrt{\frac{\beta_s^3\gamma_s^3\mu'}{\mathbf{j}\bar{k}Z_0\sigma}}\lambda I'_m(\lambda a)+I_m(\lambda a)\right)}I_m(\lambda\rho')\right]I_m(\lambda\rho), & \text{for } \rho' > \rho, \\[6mm] \left[K_m(\lambda\rho) - \dfrac{\left(-\sqrt{\frac{\beta_s^3\gamma_s^3\mu'}{\mathbf{j}\bar{k}Z_0\sigma}}\lambda K'_m(\lambda a)+K_m(\lambda a)\right)}{\left(-\sqrt{\frac{\beta_s^3\gamma_s^3\mu'}{\mathbf{j}\bar{k}Z_0\sigma}}\lambda I'_m(\lambda a)+I_m(\lambda a)\right)}I_m(\lambda\rho)\right]I_m(\lambda\rho'), & \text{for } \rho' < \rho. \end{cases} \tag{55}$$

In these expressions, $I_m(z)$ and $K_m(z)$ are the modified Bessel functions [20], the prime of $I'_m(z)$ and $K'_m(z)$ means the derivative with respect to z, $\epsilon_m = 2 - \delta_{m0}$ where δ_{mn} is the Kronecker-δ, and $\vec{r} = (\rho, \varphi, \bar{z})$, $\vec{r}' = (\rho', \varphi', \bar{z}')$.

Importantly, the Green's function in Eq. (54) satisfies the relationship:

$$G(x,y,\bar{z})|_{\rho=a} = \sqrt{\frac{\beta_s^3\gamma_s^3\mu'}{\mathbf{j}\bar{k}Z_0\sigma}}\frac{\partial G}{\partial\rho}\bigg|_{\rho=a}, \tag{56}$$

which ensures that the solved potential utilizing the Green's function adheres to the specified boundary condition.

Particularly, when the conductivity σ is infinite, Eq. (55) simplifies to

$$\mathcal{F}_m^{(inf)}(\rho;\rho') = \begin{cases} \left[K_m(\lambda\rho') - \frac{K_m(\lambda a)}{I_m(\lambda a)}I_m(\lambda\rho')\right]I_m(\lambda\rho), & \text{for } \rho' > \rho, \\ \left[K_m(\lambda\rho) - \frac{K_m(\lambda a)}{I_m(\lambda a)}I_m(\lambda\rho)\right]I_m(\lambda\rho'), & \text{for } \rho' < \rho. \end{cases} \tag{57}$$

This expression reproduces the Green's function with a perfectly conductive boundary, which was employed for the computation of the transverse space-charge impedance in Ref. [21].

The solution to the Poisson equation [Eq. (40)], which satisfies the given boundary condition, can be expressed as

$$\begin{aligned}
\bar{\Phi}(\rho,\varphi,\bar{z}) &= \int_{-\infty}^{\infty} d\bar{k} \sum_{m=0}^{\infty} \frac{cZ_0\epsilon_m}{2\pi^2} \int_0^{\rho} \rho' d\rho' \int_0^{2\pi} d\varphi' \, \cos m(\varphi-\varphi') \int_{-\infty}^{\infty} dz' \int_0^{\infty} d\lambda \\
&\times \left[K_m(\lambda\rho) - \frac{\left(-\sqrt{\frac{\beta_s^3\gamma_s^3\mu'}{\mathbf{j}\bar{k}Z_0\sigma}}\lambda K_m'(\lambda a) + K_m(\lambda a)\right)}{\left(-\sqrt{\frac{\beta_s^3\gamma_s^3\mu'}{\mathbf{j}\bar{k}Z_0\sigma}}\lambda I_m'(\lambda a) + I_m(\lambda a)\right)} I_m(\lambda\rho)\right] \\
&\times I_m(\lambda\rho') \cos[\lambda(\bar{z}-\bar{z}')]eN_b \frac{e^{-\frac{(\rho'\cos\varphi'-r_0\cos\theta_0)^2+(\rho'\sin\varphi'-r_0\sin\theta_0)^2}{2\sigma_x^2}}}{2\pi\sigma_x^2} \frac{e^{-\mathbf{j}\bar{k}\bar{z}'}}{2\pi} e^{-\frac{1}{2}\bar{k}^2\bar{\sigma}_z^2} \\
&+ \int_{-\infty}^{\infty} d\bar{k} \sum_{m=0}^{\infty} \frac{cZ_0\epsilon_m}{2\pi^2} \int_{\rho}^{\Lambda} \rho' d\rho' \int_0^{2\pi} d\varphi \, \cos m(\varphi-\varphi') \int_{-\infty}^{\infty} dz' \int_0^{\infty} d\lambda \\
&\times \left[K_m(\lambda\rho') - \frac{\left(-\sqrt{\frac{\beta_s^3\gamma_s^3\mu'}{\mathbf{j}\bar{k}Z_0\sigma}}\lambda K_m'(\lambda a) + K_m(\lambda a)\right)}{\left(-\sqrt{\frac{\beta_s^3\gamma_s^3\mu'}{\mathbf{j}\bar{k}Z_0\sigma}}\lambda I_m'(\lambda a) + I_m(\lambda a)\right)} I_m(\lambda\rho')\right] \\
&\times I_m(\lambda\rho) \cos[\lambda(\bar{z}-\bar{z}')]eN_b \frac{e^{-\frac{(\rho'\cos\varphi'-r_0\cos\theta_0)^2+(\rho'\sin\varphi'-r_0\sin\theta_0)^2}{2\sigma_x^2}}}{2\pi\sigma_x^2} \frac{e^{-\mathbf{j}\bar{k}\bar{z}'}}{2\pi} e^{-\frac{1}{2}\bar{k}^2\bar{\sigma}_z^2},
\end{aligned} \tag{58}$$

using Eq. (54). Here, the upper limit of integration over ρ' is denoted as Λ, based on the assumption that the beam is primarily confined within the region $\rho < \Lambda$, and the contribution from the Gaussian distribution's tail component ($\rho > \Lambda$) is negligible in the transverse direction.

In order to carry out the integrations over ρ', φ', z', and λ in Eq. (58), we can redefine the function $\mathcal{F}_m(\rho;\rho')$ from Eq. (55) using Bessel functions $J_m(x)$ [20,22], resulting in

$$\mathcal{F}_m(\rho;\rho') = \sum_{j=1}^{\infty} \frac{2}{a^2} \frac{J_m(\xi_{m,j}\rho)}{[J_m'(\xi_{m,j}a)]^2} \left[\frac{J_m(\xi_{m,j}\rho')}{(\lambda^2+\xi_{m,j}^2)} + \frac{\sqrt{\frac{\beta_s^3\gamma_s^3\mu'}{\mathbf{j}\bar{k}Z_0\sigma}}\xi_{m,j}I_m[\lambda\rho']J_m'[a\xi_{m,j}]}{(\lambda^2+\xi_{m,j}^2)(I_m[a\lambda] - \sqrt{\frac{\beta_s^3\gamma_s^3\mu'}{\mathbf{j}\bar{k}Z_0\sigma}}\lambda I_m'[a\lambda])}\right], \tag{59}$$

where the prime in $J_m'(z)$ denotes the derivative with respect to z. This new expression for $\mathcal{F}_m(\rho;\rho')$ utilizes the relationship:

$$\int_0^a d\rho\rho J_m(\xi_{m,j}\rho)\mathcal{F}_m(\rho;\rho') = \frac{J_m(\xi_{m,j}\rho')}{(\lambda^2+\xi_{m,j}^2)} + \frac{\sqrt{\frac{\beta_s^3\gamma_s^3\mu'}{\mathbf{j}\bar{k}Z_0\sigma}}\xi_{m,j}I_m[\lambda\rho']J_m'[a\xi_{m,j}]}{(\lambda^2+\xi_{m,j}^2)(I_m[a\lambda] - \sqrt{\frac{\beta_s^3\gamma_s^3\mu'}{\mathbf{j}\bar{k}Z_0\sigma}}\lambda I_m'[a\lambda])}. \tag{60}$$

In this context, Bessel function $J_m(z)$ satisfies the characteristic property:

$$\int_0^a d\rho\rho J_m(\xi_{m,i}\rho)\rho J_m(\xi_{m,j}\rho) = \frac{a^2}{2}[J_m'(\xi_{m,i}a)]^2\delta_{ij}, \tag{61}$$

where $a\xi_{m,j}$ represents the jth zero of the Bessel function of order m, i.e., $J_m(a\xi_{m,j}) = 0$.

The summations over index j in the first and second terms of Eq. (59) are computed as follows:

in the first term,

$$\sum_{j=1}^{\infty}\frac{2}{a^2}\frac{J_m(\xi_{m,j}\rho)}{[J'_m(\xi_{m,j}a)]^2}\frac{J_m(\xi_{m,j}\rho')}{(\lambda^2+\xi_{m,j}^2)} = \begin{cases} \left[K_m(\lambda\rho')-\frac{K_m(\lambda a)}{I_m(\lambda a)}I_m(\lambda\rho')\right]I_m(\lambda\rho), & \text{for } \rho' > \rho, \\ \left[K_m(\lambda\rho)-\frac{K_m(\lambda a)}{I_m(\lambda a)}I_m(\lambda\rho)\right]I_m(\lambda\rho'), & \text{for } \rho > \rho', \end{cases} \tag{62}$$

and in the second term,

$$\frac{2\sqrt{\frac{\beta_s^3\gamma_s^3\mu'}{\mathbf{j}kZ_0\sigma}}I_m[\lambda\rho']}{a^2(I_m[a\lambda]-\sqrt{\frac{\beta_s^3\gamma_s^3\mu'}{\mathbf{j}kZ_0\sigma}}\lambda I'_m[a\lambda])}\sum_{j=1}^{\infty}\frac{J_m(\xi_{m,j}\rho)}{J'_m(\xi_{m,j}a)}\frac{\xi_{m,j}}{(\lambda^2+\xi_{m,j}^2)}$$

$$= \begin{cases} \left[\frac{K_m(\lambda a)}{I_m(\lambda a)}I_m(\lambda\rho')-\frac{\left(-\sqrt{\frac{\beta_s^3\gamma_s^3\mu'}{\mathbf{j}kZ_0\sigma}}\lambda K'_m(\lambda a)+K_m(\lambda a)\right)}{\left(-\sqrt{\frac{\beta_s^3\gamma_s^3\mu'}{\mathbf{j}kZ_0\sigma}}\lambda I'_m(\lambda a)+I_m(\lambda a)\right)}I_m(\lambda\rho')\right]I_m(\lambda\rho), & \text{for } \rho' > \rho, \\[4mm] \left[\frac{K_m(\lambda a)}{I_m(\lambda a)}I_m(\lambda\rho)-\frac{\left(-\sqrt{\frac{\beta_s^3\gamma_s^3\mu'}{\mathbf{j}kZ_0\sigma}}\lambda K'_m(\lambda a)+K_m(\lambda a)\right)}{\left(-\sqrt{\frac{\beta_s^3\gamma_s^3\mu'}{\mathbf{j}kZ_0\sigma}}\lambda I'_m(\lambda a)+I_m(\lambda a)\right)}I_m(\lambda\rho)\right]I_m(\lambda\rho'), & \text{for } \rho' < \rho. \end{cases} \tag{63}$$

This is due to the fact that the function $\mathcal{F}_m^{(\text{inf})}(\rho;\rho')$ described by Eq. (57), which is identical to the right-hand side of Eq. (62), corresponding to the perfectly conductive boundary case, can be transformed into the left-hand side of Eq. (62) using the following relation:

$$\int_0^a d\rho\rho J_m(\xi_{m,l}\rho)\mathcal{F}_m(\rho;\rho') = \frac{J_m(\xi_{m,l}\rho')}{(\lambda^2+\xi_{m,l}^2)}. \tag{64}$$

Upon substituting Eq. (59) into Eq. (58), the scalar potential can be simplified as follows:

$$\bar{\Phi}(\rho,\varphi,\bar{z}) = \Re\left\{\sum_{j=1}^{\infty}\int_0^{\infty}d\bar{k}\sum_{m=0}^{\infty}\frac{cZ_0\epsilon_m}{\pi^2}\int_0^{\Lambda}\rho'd\rho'I_m\left(\frac{\rho'r_0}{\sigma_x^2}\right)\cos[m(\varphi-\theta_0)]\right.$$

$$\times\frac{e^{-\mathbf{j}\bar{k}\bar{z}}}{a^2}eN_b\frac{e^{-\frac{(\rho'^2+r_0^2)}{2\sigma_x^2}}}{\sigma_x^2}e^{-\frac{1}{2}\bar{k}^2\bar{\sigma}_z^2}\frac{J_m(\xi_{m,j}\rho)}{[J'_m(\xi_{m,j}a)]^2}$$

$$\left.\times\left[\frac{J_m(\xi_{m,j}\rho')}{(\bar{k}^2+\xi_{m,j}^2)}+\frac{\sqrt{\frac{\beta_s^3\gamma_s^3\mu'}{\mathbf{j}\bar{k}Z_0\sigma}}\xi_{m,j}I_m[\bar{k}\rho']J'_m[a\xi_{m,j}]}{(\bar{k}^2+\xi_{m,j}^2)(I_m[a\bar{k}]-\sqrt{\frac{\beta_s^3\gamma_s^3\mu'}{\mathbf{j}\bar{k}Z_0\sigma}}\bar{k}I'_m[a\bar{k}])}\right]\right\}. \tag{65}$$

The integration with respect to φ' can be performed using the formula:

$$\int_0^{2\pi}d\varphi'\cos m(\varphi-\varphi')e^{\frac{\rho'r_0\cos(\varphi'-\theta_0)}{\sigma_x^2}} = 2\pi I_m\left(\frac{\rho'r_0}{\sigma_x^2}\right)\cos[m(\varphi-\theta_0)]. \tag{66}$$

In order to carry out the integration with respect to ρ' in Eq. (65), we need to expand the product of the Bessel functions for their arguments as follows [22]:
for the term involving $J_m(\xi_{m,j}\rho')I_m(\frac{r_0}{\sigma_x^2}\rho')$:

$$J_m(\xi_{m,j}\rho')I_m\left(\frac{r_0}{\sigma_x^2}\rho'\right) = \sum_{n=0}^{\infty}\rho'^{2n+2m}\frac{(-1)^n\xi_{m,j}^{2n+m}r_0^m{}_2F_1\left[-m-n,-n,1+m,-\frac{r_0^2}{\sigma_x^4\xi_{m,j}^2}\right]}{\sigma_x^{2m}4^{n+m}n!m!(m+n)!}, \tag{67}$$

and for the term involving $I_m(\bar{k}\rho')I_m(\frac{r_0}{\sigma_x^2}\rho')$:

$$I_m(\bar{k}\rho')I_m\left(\frac{r_0}{\sigma_x^2}\rho'\right) = \sum_{n=0}^{\infty} \rho'^{2n+2m} \frac{\bar{k}^{2n+m}r_0^m\, _2F_1\left[-m-n,-n,1+m,\frac{r_0^2}{\sigma_x^4\bar{k}^2}\right]}{\sigma_x^{2m}4^{n+m}n!m!(m+n)!}, \tag{68}$$

where $_2F_1[\alpha,\beta,\gamma;z]$ represents Gaussian hypergeometric function [20,23,24].

Ultimately, we arrive at the following expression:

$$\begin{aligned}
\bar{\Phi}(\rho,\varphi,\bar{z}) = \Re\Bigg\{ & \sum_{n=0}^{\infty}\sum_{j=1}^{\infty}\int_0^{\infty} d\bar{k} \sum_{m=0}^{\infty} \frac{cZ_0\epsilon_m}{\pi^2}\cos[m(\varphi-\theta_0)] \\
& \times \frac{e^{-\mathbf{j}\bar{k}\bar{z}}}{a^2}eN_b e^{-\frac{r_0^2}{2\sigma_x^2}}e^{-\frac{1}{2}\bar{k}^2\bar{\sigma}_z^2}\frac{J_m(\xi_{m,j}\rho)}{[J'_m(\xi_{m,j}a)]^2}\sigma_x^{2n}\left((m+n)! - \Gamma\left[1+m+n,\frac{\Lambda^2}{2\sigma_x^2}\right]\right) \\
& \times \left[\frac{1}{(\bar{k}^2+\xi_{m,j}^2)}\frac{(-1)^n\xi_{m,j}^{2n+m}r_0^m\, _2F_1\left[-m-n,-n,1+m,-\frac{r_0^2}{\sigma_x^4\xi_{m,j}^2}\right]}{2^{n+m}n!m!(m+n)!}\right. \\
& \left. +\frac{\sqrt{\frac{\beta_s^3\gamma_s^3\mu'}{\mathbf{j}\bar{k}Z_0\sigma}}\xi_{m,j}J'_m[a\xi_{m,j}]}{(\bar{k}^2+\xi_{m,j}^2)(I_m[a\bar{k}]-\sqrt{\frac{\beta_s^3\gamma_s^3\mu'}{\mathbf{j}\bar{k}Z_0\sigma}}\bar{k}I'_m[a\bar{k}])}\frac{\bar{k}^{2n+m}r_0^m\, _2F_1[-m-n,-n,1+m,\frac{r_0^2}{\sigma_x^4\bar{k}^2}]}{2^{n+m}n!m!(m+n)!}\right]\Bigg\}.
\end{aligned} \tag{69}$$

This expression is obtained through integration with respect to φ', utilizing the relation:

$$\int_0^{\Lambda} d\rho' e^{-\frac{\rho'^2}{2\sigma_x^2}}\rho'^{2n+2m+1} = 2^{(m+n)}\sigma_x^{2(m+n)}\sigma_x^2\left((m+n)! - \Gamma\left[1+m+n,\frac{\Lambda^2}{2\sigma_x^2}\right]\right), \tag{70}$$

where $\Gamma[a,z]$ refers to the incomplete Gamma function [20].

To verify the consistency of the present formalism with the approach based on mirror currents for handling the chamber boundary, let us consider the limit as σ_x tends to zero and the conductivity σ approaches infinity in Eq. (69). In the limit, Eq. (69) simplifies to

$$\lim_{\sigma_x\to 0,\sigma\to\infty}\bar{\Phi}(\rho,\varphi,\bar{z}) = \Re\left\{\int_0^{\infty} d\bar{k}\sum_{m=0}^{\infty}\frac{cZ_0\epsilon_m}{\pi^2}\cos[m(\varphi-\theta_0)]\frac{e^{-\mathbf{j}\bar{k}\bar{z}}}{a^2}eN_b e^{-\frac{1}{2}\bar{k}^2\bar{\sigma}_z^2}\frac{r_0^m}{2^m m!}\sum_{j=1}^{\infty}\frac{J_m(\xi_{m,j}\rho)}{[J'_m(\xi_{m,j}a)]^2}\frac{\xi_{m,j}^m}{(\bar{k}^2+\xi_{m,j}^2)}\right\}, \tag{71}$$

after employing:

$$\lim_{\sigma_x\to 0}{_2F_1}\left[-m-n,-n,1+m,-\frac{r_0^2}{\sigma_x^4\xi_{m,j}^2}\right] = \left(-\frac{r_0^2}{\sigma_x^4\xi_{m,j}^2}\right)^n, \tag{72}$$

$$\lim_{\Lambda\to\infty}\Gamma\left[1+m+n,\frac{\Lambda^2}{2\sigma_x^2}\right] = 0. \tag{73}$$

The summation over j in Eq. (71) can be further performed as

$$\lim_{\sigma_x\to 0,\sigma\to\infty}\bar{\Phi}(\rho,\varphi,\bar{z}) = \Re\left\{\int_0^{\infty} d\bar{k}\sum_{m=0}^{\infty}\frac{cZ_0\epsilon_m}{2\pi^2}\cos[m(\varphi-\theta_0)]e^{-\mathbf{j}\bar{k}\bar{z}}eN_b e^{-\frac{1}{2}\bar{k}^2\bar{\sigma}_z^2}\frac{\bar{k}^m r_0^m}{2^m m!}\left[K_m(\bar{k}\rho)-\frac{K_m(\bar{k}a)}{I_m(\bar{k}a)}I_m(\bar{k}\rho)\right]\right\}, \tag{74}$$

by utilizing

$$\sum_{j=1}^{\infty} \frac{J_m(\xi_{m,j}\rho)}{[J'_m(\xi_{m,j}a)]^2} \frac{\xi_{m,j}^m}{(\bar{k}^2 + \xi_{m,j}^2)} = \left[K_m(\bar{k}\rho) - \frac{K_m(\bar{k}a)}{I_m(\bar{k}a)} I_m(\bar{k}\rho) \right] \bar{k}^m \frac{a^2}{2},$$ (75)

which is derived from Eq. (62) for $\rho > \rho'$ after taking a limit for infinitesimal ρ'.

Finally, adhering to the methodology elucidated in Sec. II for obtaining the scalar potential of a coasting beam, we perform the integration of Eq. (74) with respect to z_i over the range from negative infinity to positive infinity.

This process entails substituting $\bar{z}$ with $\bar{z} - z_i$ in Eq. (74) and subsequently dividing the outcome by the circumference $2\pi R$ following the transformation of the scalar potential from the rest frame to the laboratory frame. The outcome is the two-dimensional scalar potential $\Phi_{2D}(x, y)$ in the laboratory frame:

$$\begin{aligned}
\Phi_{2D}(x, y) &= \lim_{\sigma_x \to 0, \sigma \to \infty} \frac{\gamma_s}{2\pi R} \int_{-\infty}^{\infty} dz_i \bar{\Phi}[\rho, \varphi, \gamma_s(\bar{z} - z_i)] \\
&= \lim_{\sigma_x \to 0, \sigma \to \infty} \frac{1}{2\pi R} \int_{-\infty}^{\infty} dz_i \Phi(\rho, \varphi, \bar{z} - z_i) \\
&= \frac{\gamma_s}{2\pi R} \int_{-\infty}^{\infty} dz_i \Re \left\{ \int_0^{\infty} d\bar{k} \sum_{m=0}^{\infty} \frac{cZ_0 \epsilon_m}{2\pi^2} \cos[m(\varphi - \theta_0)] \right. \\
&\quad \left. \times e^{-j\bar{k}\gamma_s(\bar{z} - z_i)} e N_b e^{-\frac{1}{2}\bar{k}^2\gamma_s^2\sigma_{\bar{z}}^2} \frac{\bar{k}^m r_0^m}{2^m m!} \left[K_m(\bar{k}\rho) - \frac{K_m(\bar{k}a)}{I_m(\bar{k}a)} I_m(\bar{k}\rho) \right] \right\} \\
&= -\tilde{\lambda} \frac{cZ_0}{\pi} \log\left[\frac{\rho}{a}\right] + \tilde{\lambda} \frac{2cZ_0}{\pi} \sum_{m=1}^{\infty} \frac{\cos[m(\varphi - \theta_0)]}{2m} \left[\left(\frac{r_0}{\rho}\right)^m - \left(\frac{r_0 \rho}{a^2}\right)^m \right],
\end{aligned}$$ (76)

$$= -\tilde{\lambda} \frac{cZ_0}{2\pi} \log\left[\frac{a^2}{(x_0^2 + y_0^2)}\right] - \tilde{\lambda} \frac{cZ_0}{2\pi} \log\left[\frac{[(x - x_0)^2 + (y - y_0)^2]}{\left[\left(x - \frac{a^2 x_0}{(x_0^2 + y_0^2)}\right)^2 + \left(y - \frac{a^2 y_0}{(x_0^2 + y_0^2)}\right)^2\right]} \right],$$ (77)

where $\tilde{\lambda}$ represents the line density. Here, we employ the relation:

$$\sum_{m=1}^{\infty} \frac{a^m \cos(m\theta)}{2m} = -\frac{1}{4} \log[1 + a^2 - 2a\cos(\theta)],$$ (78)

to perform the summation over m in Eq. (76).

Ultimately, we can establish that Eq. (77) is equivalent to Eq. (31) obtained using a mirror current, except for a constant term related to the derivative of x (the first term in Eq. (77)). This additional term guarantees that $\Phi_{2D}(x, y) = 0$ at the chamber boundary surface, where $\rho = a$.

Having confirmed the consistency of the current formalism with the mirror currents approach, the following subsections will involve the computation of both coherent and incoherent tune shifts for a bunched beam constrained within a conductive cylindrical chamber, starting with Eq. (69). Subsequently, we will assess the consistency of these results by comparing them with previous findings. Furthermore, we will explore the influence of material properties on these tune shifts.

A. Coherent tune shift

To calculate the horizontal coherent tune shift, we evaluate:

$$\begin{aligned}
&\frac{\partial^2 \bar{\Phi}(\rho, \varphi, \bar{z})}{\partial x^2} + \frac{\partial^2 \bar{\Phi}(\rho, \varphi, \bar{z})}{\partial x_0 \partial x}\bigg|_{\varphi=\theta_0, \rho=r_0=0, \bar{z}=0} \\
&= \left(\frac{\partial^2 \bar{\Phi}^{(1)}(\rho, \varphi, \bar{z})}{\partial x^2} + \frac{\partial^2 \bar{\Phi}^{(1)}(\rho, \varphi, \bar{z})}{\partial x_0 \partial x}\bigg|_{\varphi=\theta_0, \rho=r_0=0, \bar{z}=0} \right) \\
&\quad + \left(\frac{\partial^2 \bar{\Phi}^{(2)}(\rho, \varphi, \bar{z})}{\partial x^2} + \frac{\partial^2 \bar{\Phi}^{(2)}(\rho, \varphi, \bar{z})}{\partial x_0 \partial x}\bigg|_{\varphi=\theta_0, \rho=r_0=0, \bar{z}=0} \right),
\end{aligned}$$ (79)

utilizing Eq. (69) after applying synthetic differential for the equation. Consequently, only $m = 0$ and $m = 1$ terms in Eq. (69) are retained in the calculation. Here, the first term corresponding to the perfectly conductive chamber, and the second term accounting for correction terms due to the chamber's material properties, are, respectively, defined as

$$\frac{\partial^2 \bar{\Phi}^{(1)}(\rho,\varphi,\bar{z})}{\partial x^2} + \frac{\partial^2 \bar{\Phi}^{(1)}(\rho,\varphi,\bar{z})}{\partial x_0 \partial x}\Bigg|_{\varphi=\theta_0,\rho=r_0=0,\bar{z}=0} = -\frac{eN_b cZ_0}{4\pi a^2} \sum_{j=1}^{\infty} \frac{\xi_{0,j} e^{-\frac{\sigma_x^2 \xi_{0,j}^2}{2}}}{[J_0'(\xi_{0,j}a)]^2} e^{\frac{\xi_{0,j}^2 \bar{\sigma}_z^2}{2}} \text{Erfc}\left[\frac{\xi_{0,j}\bar{\sigma}_z}{\sqrt{2}}\right]$$

$$+ \frac{eN_b cZ_0}{4\pi a^2} \sum_{j=1}^{\infty} \frac{\xi_{1,j} e^{-\frac{\sigma_x^2 \xi_{1,j}^2}{2}}}{[J_1'(\xi_{1,j}a)]^2} e^{\frac{\xi_{1,j}^2 \bar{\sigma}_z^2}{2}} \text{Erfc}\left[\frac{\xi_{1,j}\bar{\sigma}_z}{\sqrt{2}}\right], \qquad (80)$$

and

$$\frac{\partial^2 \bar{\Phi}^{(2)}(\rho,\varphi,\bar{z})}{\partial x^2} + \frac{\partial^2 \bar{\Phi}^{(2)}(\rho,\varphi,\bar{z})}{\partial x_0 \partial x}\Bigg|_{\varphi=\theta_0,\rho=r_0=0,\bar{z}=0}$$

$$= \Re\left\{ -\frac{eN_b cZ_0}{2\pi^2 a^2} \int_0^{\infty} d\bar{k} \frac{e^{-\frac{1}{2}\bar{k}^2 \bar{\sigma}_z^2} e^{\frac{\sigma_x^2 \bar{k}^2}{2}} \sqrt{\frac{\beta_s^3 \gamma_s^3 \mu'}{\mathbf{j}kZ_0\sigma}}}{\left(I_0[a\bar{k}] - \sqrt{\frac{\beta_s^3 \gamma_s^3 \mu'}{\mathbf{j}kZ_0\sigma}}\bar{k}I_0'[a\bar{k}]\right)} \sum_{j=1}^{\infty} \frac{\xi_{0,j}^3 J_0'[a\xi_{0,j}]}{(\bar{k}^2 + \xi_{0,j}^2)[J_0'(\xi_{0,j}a)]^2} \right.$$

$$\left. + \frac{eN_b cZ_0}{2\pi^2 a^2} \int_0^{\infty} d\bar{k} \frac{e^{-\frac{1}{2}\bar{k}^2 \bar{\sigma}_z^2} e^{\frac{\sigma_x^2 \bar{k}^2}{2}} \sqrt{\frac{\beta_s^3 \gamma_s^3 \mu'}{\mathbf{j}kZ_0\sigma}}\bar{k}}{\left(I_1[a\bar{k}] - \sqrt{\frac{\beta_s^3 \gamma_s^3 \mu'}{\mathbf{j}kZ_0\sigma}}\bar{k}I_1'[a\bar{k}]\right)} \sum_{j=1}^{\infty} \frac{\xi_{1,j}^2}{(\bar{k}^2 + \xi_{1,j}^2)[J_1'(\xi_{1,j}a)]} \right\}. \qquad (81)$$

In the derivation, we assume $\Lambda \gg 2\sigma_x$ and utilize Eq. (73), the formulas:

$$\lim_{r_0 \to 0} \frac{\partial}{\partial r_0}\left(e^{-\frac{r_0^2}{2\sigma_x^2}} r_0^m {}_2F_1\left[-m-n,-n,1+m,\frac{r_0^2}{A}\right]\right) = \delta_{m,1},$$

$$\qquad (82)$$

$${}_2F_1[-m-n,-n,1+m,0] = 1, \qquad (83)$$

$$\int_0^{\infty} d\lambda \frac{e^{-\frac{\lambda^2 \bar{\sigma}_z^2}{2}}}{(\lambda^2 + \xi_{m,j}^2)} = \frac{e^{\frac{\xi_{m,j}^2 \bar{\sigma}_z^2}{2}}\pi \text{Erfc}\left[\frac{\xi_{m,j}\bar{\sigma}_z}{\sqrt{2}}\right]}{2\xi_{m,j}}, \qquad (84)$$

as well as the complementary error function Erfc[x] [20], defined as

$$\text{Erfc}[x] = \frac{2}{\sqrt{\pi}} \int_x^{\infty} e^{-t^2} dt. \qquad (85)$$

Notably, Eq. (81) approaches zero for infinite conductivity σ.

The summation over j in the correction term of Eq. (81) can be executed by employing the formulas

$$\sum_{j=1}^{\infty} \frac{\xi_{0,j}^3}{J_0'(\xi_{0,j}a)(\bar{k}^2 + \xi_{0,j}^2)} = \frac{\bar{k}^2 a}{2I_0(\bar{k}a)}, \qquad (86)$$

and

$$\sum_{j=1}^{\infty} \frac{\xi_{1,j}^2}{J_1'(\xi_{1,j}a)(\bar{k}^2 + \xi_{1,j}^2)} = -\frac{\bar{k}a}{2I_1(\bar{k}a)}. \qquad (87)$$

Equation (86) is derived by taking a derivative of

$$\sum_{j=1}^{\infty} \frac{J_m(\xi_{m,j}\rho)}{J_m'(\xi_{m,j}a)} \frac{\xi_{m,j}}{(\bar{k}^2 + \xi_{m,j}^2)} = -\frac{a\, I_m(\bar{k}\rho)}{2\, I_m(\bar{k}a)}, \qquad (88)$$

which originates from Eq. (63), with respect to ρ for $m = 0$ when ρ is infinitesimally small. Meanwhile, Eq. (87) is obtained from Eq. (88) for $m = 1$ when ρ is infinitesimally small.

As a result, Eq. (81) is further simplified as

$$\frac{\partial^2 \bar{\Phi}^{(2)}(\rho,\varphi,\bar{z})}{\partial x^2} + \frac{\partial^2 \bar{\Phi}^{(2)}(\rho,\varphi,\bar{z})}{\partial x_0 \partial x}\Bigg|_{\varphi=\theta_0,\rho=r_0=0,\bar{z}=0}$$

$$= \Re\left\{ -\frac{cZ_0}{4\pi^2}\frac{eN_b}{a} \int_0^{\infty} d\bar{k} \frac{\bar{k}^2 e^{-\frac{1}{2}\bar{k}^2 \bar{\sigma}_z^2 + \frac{\bar{k}^2 \sigma_x^2}{2}} \sqrt{\frac{\beta_s^3 \gamma_s^3 \mu'}{\mathbf{j}kZ_0\sigma}}}{I_0(\bar{k}a)\left(I_0[a\bar{k}] - \sqrt{\frac{\beta_s^3 \gamma_s^3 \mu'}{\mathbf{j}kZ_0\sigma}}\bar{k}I_0'[a\bar{k}]\right)} \right.$$

$$\left. - \frac{cZ_0}{4\pi^2}\frac{eN_b}{a} \int_0^{\infty} d\bar{k} \frac{\bar{k}^2 e^{-\frac{1}{2}\bar{k}^2 \bar{\sigma}_z^2 + \frac{\bar{k}^2 \sigma_x^2}{2}} \sqrt{\frac{\beta_s^3 \gamma_s^3 \mu'}{\mathbf{j}kZ_0\sigma}}}{I_1(\bar{k}a)\left(I_1[a\bar{k}] - \sqrt{\frac{\beta_s^3 \gamma_s^3 \mu'}{\mathbf{j}kZ_0\sigma}}\bar{k}I_1'[a\bar{k}]\right)} \right\}. \qquad (89)$$

The formulation that incorporates the zeros of the Bessel function in Eq. (80) can be understood as a method of replacing the boundary condition by utilizing the superposition of image currents at positions $\zeta_{m,j}a$ along the radial direction for the bunched beam [19]. This approach is advantageous for conducting analytical calculations. Even within the context of Eq. (89) dealing with the correction effects, the expansion of these terms related to the zeros of Bessel functions will play a crucial role in the analysis

when we make approximations to assess their impact on the coherent and incoherent tune shifts.

The contribution stemming from the direct space-charge effect is isolated from Eq. (80) by considering a limit as the chamber radius a tends toward infinity. In this scenario, the summation over j is substituted with an integration over x as shown below:

$$
\begin{aligned}
&\frac{\partial^2 \bar{\Phi}^{(1)}(\rho, \varphi, \bar{z})}{\partial x^2} + \frac{\partial^2 \bar{\Phi}^{(1)}(\rho, \varphi, \bar{z})}{\partial x_0 \partial x}\bigg|_{\varphi=\theta_0, \rho=r_0=0, \bar{z}=0} \\
&= -\int_0^\infty dx \frac{cZ_0}{8\pi} eN_b x^2 e^{-\frac{x^2\sigma_x^2}{2}} e^{\frac{x^2\bar{\sigma}_z^2}{2}} \text{Erfc}\left[\frac{x\bar{\sigma}_z}{\sqrt{2}}\right] \\
&\quad + \int_0^\infty dx \frac{cZ_0}{8\pi} eN_b x^2 e^{-\frac{x^2\sigma_x^2}{2}} e^{\frac{x^2\bar{\sigma}_z^2}{2}} \text{Erfc}\left[\frac{x\bar{\sigma}_z}{\sqrt{2}}\right] = 0,
\end{aligned}
\tag{90}
$$

where we make use of the fact that the zeros $\xi_{m,j}a$ of the Bessel function and $J'_m(\xi_{m,j}a)$ approach the following values [20,22]:

$$
\xi_{m,j}a = \frac{m\pi}{2} + \frac{3\pi}{4} + (j-m-1)\pi, \quad \text{for } j \geq 1, \text{ and } m \geq 0,
\tag{91}
$$

$$
J'_m(\xi_{m,j}a) = \sqrt{\frac{2}{\pi(\frac{m\pi}{2} + \frac{3\pi}{4} + (j-m-1)\pi)}} (-1)^{(j-m)},
\tag{92}
$$

for large a.

An interesting observation is that the cancellation occurs between the first and second terms in Eq. (80), indicating the disappearance of the coherent tune shift due to the direct space-charge effect. This finding aligns with the discussion in Sec. II and reproduces the absence of direct space-charge contribution in Eqs. (1) and (4).

Upon substituting Eq. (80) into Eq. (18), we arrive at a more precise expression for the coherent tune shift $\Delta\nu^{(1)}_{sp,coh}$ of an axisymmetric Gaussian beam within a perfectly conductive cylindrical chamber. This expression is ultimately given by

$$
\begin{aligned}
\Delta\nu^{(1)}_{sp,coh} = &-\frac{R^2 r_p N_b}{2\nu_{T,0} a^3 \beta_s^2 \gamma_s^2} \\
&\times \sum_{j=1}^\infty \Bigg[\frac{(\xi_{0,j}a) e^{\frac{(\xi_{0,j}a)^2(\gamma_s^2\sigma_z^2 - \sigma_x^2)}{2a^2}} \text{Erfc}\left[\frac{(\xi_{0,j}a)\gamma_s\sigma_z}{\sqrt{2}a}\right]}{[J'_0(\xi_{0,j}a)]^2} \\
&\quad - \frac{(\xi_{1,j}a) e^{\frac{(\xi_{1,j}a)^2(\gamma_s^2\sigma_z^2 - \sigma_x^2)}{2a^2}} \text{Erfc}\left[\frac{(\xi_{1,j}a)\gamma_s\sigma_z}{\sqrt{2}a}\right]}{[J'_1(\xi_{1,j}a)]^2} \Bigg].
\end{aligned}
\tag{93}
$$

The expression in Eq. (93) sheds light on the critical dependence of Lorentz-β_s and $-\gamma_s$ on the tune shift through

beam parameters (σ_z, σ_x). This stands in contrast to formula (4).

In the case of a typical relativistic beam, where

$$
\pi \frac{\gamma_s \sigma_z}{\sqrt{2}a} \gg 1,
\tag{94}
$$

Eq. (93) can be further simplified to

$$
\begin{aligned}
\Delta\nu^{(1)}_{sp,coh} = &-\frac{r_p(n_b N_b) R}{2\pi\nu_{T,0} a^2 \left(\frac{n_b\sqrt{2\pi}\sigma_z}{2\pi R}\right) \beta_s^2 \gamma_s^3} \\
&\times \sum_{j=1}^\infty \left[\frac{e^{-\frac{(\xi_{0,j}a)^2\sigma_x^2}{2a^2}}}{[J'_0(\xi_{0,j}a)]^2} - \frac{e^{-\frac{(\xi_{1,j}a)^2\sigma_x^2}{2a^2}}}{[J'_1(\xi_{1,j}a)]^2} \right].
\end{aligned}
\tag{95}
$$

This simplification arises from the utilization of the approximation

$$
e^{x^2}\text{Erfc}[x] \simeq \frac{1}{\sqrt{\pi}x},
\tag{96}
$$

for $x \gg 1$.

Equation (95) evidently exhibits a proportional relationship with $1/\beta_s^2\gamma_s^3$, which is consistent with formula (4). Moreover, Eq. (95) approaches formula (4) for the infinitesimal σ_x. In the reproduction, a sophisticated procedure is employed, utilizing

$$
\frac{d}{d\rho} \sum_{j=1}^\infty \frac{J_0(\xi_{0,j}\rho)}{[J'_0(\xi_{0,j}a)]^2 \xi_{0,j}^2} = -\sum_{j=1}^\infty \frac{J_1(\xi_{0,j}\rho)}{[J'_0(\xi_{0,j}a)]^2 \xi_{0,j}} = -\frac{a^2}{2\rho},
\tag{97}
$$

which is derived after applying Eq. (75) at the limit of $\bar{k} = 0$ for $m = 0$, and

$$
\sum_{j=1}^\infty \frac{J_1(\xi_{1,j}\rho)}{[J'_1(\xi_{1,j}a)]^2 \xi_{1,j}} = \frac{(a^2 - \rho^2)}{2\rho},
\tag{98}
$$

which is obtained after applying the expression for $m = 1$ and then taking the summation of Eqs. (97) and (98) before taking a limit as ρ becomes zero.

However, in order to rigorously account for the Lorentz-β_s and $-\gamma_s$ dependence during the acceleration process, it becomes necessary to consider the adiabatic damping effects on both the transverse bunch size and the bunch length. Consequently, we introduce normalized transverse emittance ϵ_N and longitudinal emittance J_{L0} to represent σ_x and bunch length σ_z, respectively, as follows [9]:

$$
\sigma_x = \sqrt{\frac{\epsilon_N \langle \beta_x \rangle}{\beta_s \gamma_s}},
\tag{99}
$$

$$\sigma_z = \left(\frac{2RJ_{L0}|\eta|c}{\beta_s \gamma_s \nu_{s0} m_p c^2/e} \right)^{\frac{1}{2}} = \left(\frac{8\pi R^2 J_{L0}^2 c^2 |\eta|}{h\gamma_s V \cos\phi_s m_p c^2/e} \right)^{\frac{1}{4}},$$

$$(100)$$

where ν_{s0} denotes the synchrotron tune:

$$\nu_{s0} = \frac{1}{\beta_s} \sqrt{\frac{h|\eta|V\cos\phi_s}{2\pi\gamma_s m_p c^2/e}},$$

$$(101)$$

and η represents the slippage factor:

$$\eta = \alpha - \frac{1}{\gamma_s^2}.$$

$$(102)$$

Here, α signifies the momentum compaction factor, h stands for the harmonic number, ϕ_s is the synchronous phase, and V corresponds to the acceleration voltage.

We will now perform a detailed comparison between Eqs. (1), (4), (93), and (95) (after substituting $\eta_b = 0$) across different parameter regions. In Fig. 1, we can observe the pattern of ramping over a 20-ms interval for both the synchronous phase ϕ_s and the acceleration voltage V, which are typical parameters implemented into the Rapid Cycling Synchrotron in J-PARC [25]. Meanwhile, the corresponding representation of Lorentz-β_s and -γ_s during the acceleration is depicted in Fig. 2. This scenario involves a proton beam with a normalized transverse emittance of $\epsilon_N = 2 \times 10^{-5}$ m, a total of two bunches, a harmonic number of $h = 2$, an average transverse beta function of $\langle\beta_x\rangle = 8.58$ m, an accelerator radius of $R = 55.4$ m, the chamber radius is $a = 0.145$ m, the nominal tune is $\nu_{T,0} = 6.45$, and the momentum compaction factor is $\alpha = 0.0124619$.
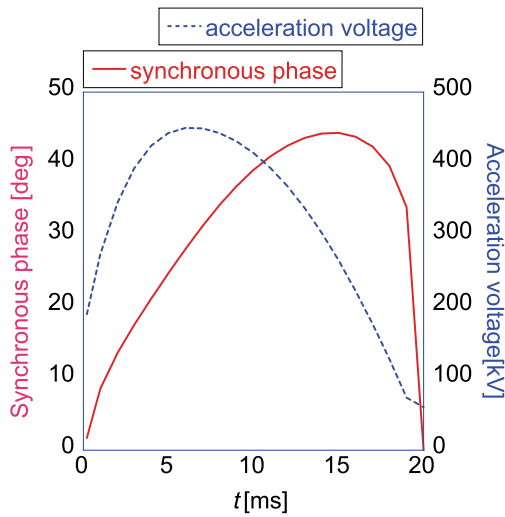

FIG. 1. The synchronous phase ϕ_s (red) and the acceleration voltage V (blue) for the pattern of ramping. The left and right axes denote the scales for ϕ_s and V, respectively.
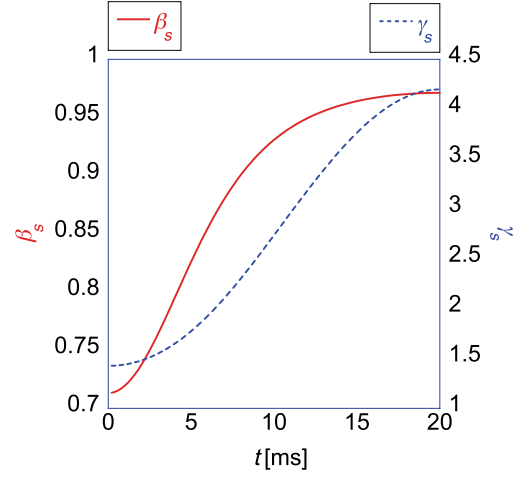

FIG. 2. The changes in Lorentz-β_s (red) and -γ_s (blue) throughout the acceleration phase. The left and right axes denote the scales for β_s and γ_s, respectively.

In the left panel in Fig. 3, the space-charge tune shifts are displayed for a bunch with a normalized longitudinal emittance of $V_{L0} = 3.4545$ Vs, containing a total of $N_b = 4.15 \times 10^{13}$ particles. The lines in different colors, namely green dashed (Laslett), black dot with "×" (Zötter), red solid with "○" (rigorous), and blue dashed with "□" (approximate), correspond to the results derived from Eqs. (1), (4), (93), and (95), respectively. The middle and right panels display the variation of the left-hand side $(\pi\gamma_s\sigma_z/\sqrt{2}a)$ of Eq. (94) and $(\beta_s^2\gamma_s^2 B)$ as they relate to different Lorentz-β_s values.

As observed in the middle and right panels, the results pertain to a scenario characterized by a relativistic and elongated bunch. The approximate formula (95) aligns well with the rigorous formula (93) thanks to the relativistic approximation. Meanwhile, formula (4) provides a good approximation to the precise results as it is derived based on the assumption of a coasting beam. Consequently, all outcomes are in good agreement, except for the result obtained using formula (1) for a thin chamber, which deviates significantly from formula (4) for a thick chamber because $(\beta_s^2\gamma_s^2 B)$ is notably larger than 1.

Figure 4 deals with shorter bunch cases with $N_b = 2.075 \times 10^{12}$. The middle and right panels display the variation of the left-hand side $(\pi\gamma_s\sigma_z/\sqrt{2}a)$ of Eq. (94) and $(\beta_s^2\gamma_s^2 B)$ through alterations in the longitudinal emittance J_{L0}. On the left panel, we present the space-charge tune shifts for various values, as seen in the middle and right panels of Fig. 4. In the graphs, the dot with "◇" (Zötter), solid (rigorous), and dashed marked with "○" (approximation) lines represent calculations based on Eqs. (4), (93), and (95), respectively. The colors used in all panels correspond to the same conditions used for calculating the space-charge tune shifts. As demonstrated in the right panel, $1 + \beta_s^2\gamma_s^2 B$ is close to 1. Therefore, in this
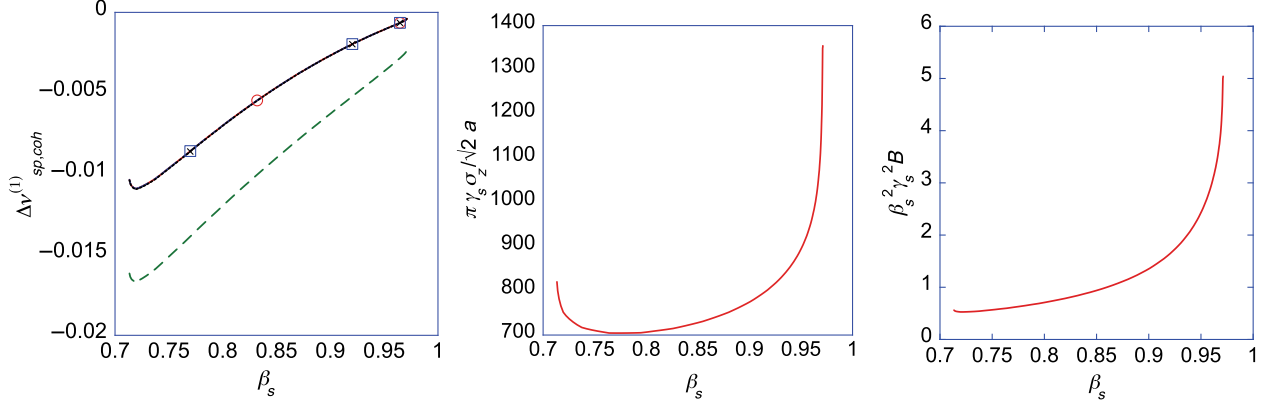
FIG. 3. On the left side, we present the space charge tune shifts. The lines in green dashed (Laslett), black dot with '×' (Zötter), red solid with '○' (rigorous), and blue dashed with '□' (approximate) correspond to Eqs. (1), (4), (93), and (95), respectively. The middle and right panels display the variation of the left-hand side of Eq. (94) and $(\beta_s^2\gamma_s^2B)$ as they relate to different Lorentz-β_s values.

case, the results from Eq. (1) (Laslett) are omitted since they closely overlap with the results from Eq. (4).

Once again, it is noteworthy that the dashed lines, denoted by "○" and derived from Eq. (95), provide a suitable approximation to the rigorous results obtained from Eq. (93), especially when the left-hand side $(\pi\gamma_s\sigma_z/\sqrt{2}a)$ of Eq. (94) increases in magnitude. This observation is evident in the black solid line and the black

dashed line marked with "○". The overlap of the approximate results calculated by Eqs. (4) and (95), facilitated by the product of $\gamma_s\sigma_z$ in formula (93), is apparent for all cases. However, they exhibit significant deviations from the rigorous results (solid lines) for nonrelativistic shorter bunch cases, as indicated by the red and blue lines.

The ratio R_0, defined as the exact formula (93) divided by formula (95),

$$R_0\left(x=\frac{\sigma_x}{\sqrt{2}a},z=\frac{\gamma_s\sigma_z}{\sqrt{2}a}\right)=\sqrt{\pi}z\frac{\sum_{j=1}^{\infty}\left[\frac{(\xi_{0,j}a)e^{(\xi_{0,j}a)^2(z^2-x^2)}\mathrm{Erfc}[(\xi_{0,j}a)z]}{[J_0'(\xi_{0,j}a)]^2}-\frac{(\xi_{1,j}a)e^{(\xi_{1,j}a)^2(z^2-x^2)}\mathrm{Erfc}[(\xi_{1,j}a)z]}{[J_1'(\xi_{1,j}a)]^2}\right]}{\sum_{j=1}^{\infty}\left[\frac{e^{-(\xi_{0,j}a)^2x^2}}{[J_0'(\xi_{0,j}a)]^2}-\frac{e^{-(\xi_{1,j}a)^2x^2}}{[J_1'(\xi_{1,j}a)]^2}\right]},\qquad(103)$$

provides a useful guideline to judge whether the relativistic or coasting approximation is suitable to describe the coherent tune shift. Let us investigate the behavior of $R_0(x,z)$ along $z=\gamma_s\sigma_z/\sqrt{2}a$ for various normalized transverse beam sizes

x, as shown in Fig. 5. The lines in red with "○", blue dashed with "□", black dot with "◇", green dot with "×", and purple solid with "×" correspond to the cases of $x(=\sigma_x/\sqrt{2}a)=0.028,\ 0.056,\ 0.085,\ 0.113,$ and $0.141,$
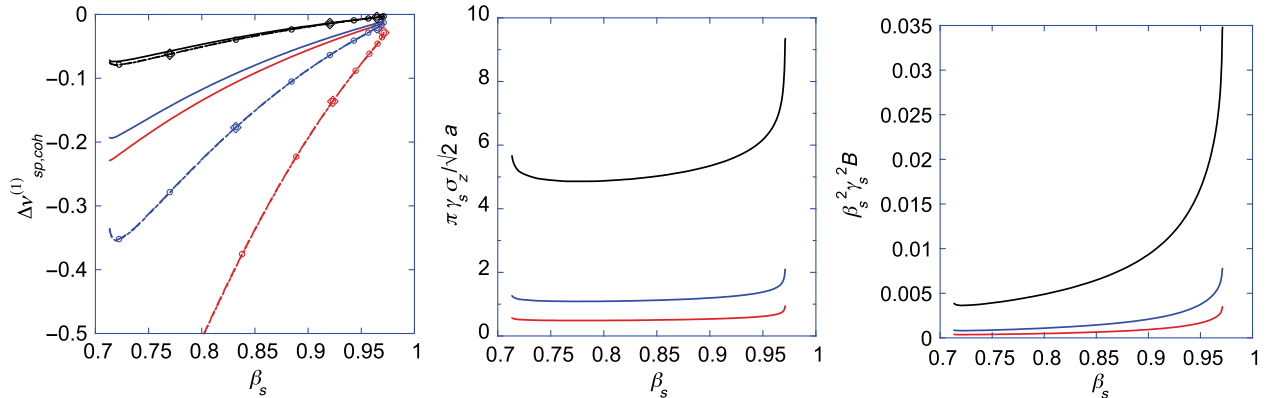

FIG. 4. On the left panel, we present the space-charge tune shifts for various values on the left-hand side of Eq. (94) (middle), using a total particle count of $N_b=2.075\times10^{12}$, where the dot with "◇" (Zötter), solid (rigorous), and dashed marked with "○" (approximation) lines represent calculations made using Eqs. (4), (93), and (95), respectively. The right panel shows $(\beta_s^2\gamma_s^2B)$ for various values corresponding to the condition in the middle panel. The colors used in all panels correspond to the same conditions employed for calculating the space-charge tune shifts.
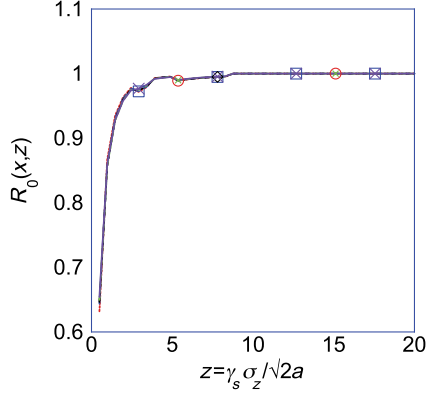
FIG. 5. The variation of function $R_0(x, z)$ along z. The lines in red with "∘", blue dashed with "□", black dot with "⋄", green dot with "×", and purple solid with "×" correspond to the cases of $x(= \sigma_x/\sqrt{2}a) = 0.028, 0.056, 0.085, 0.113$, and 0.141, respectively.

respectively. All results almost overlap, demonstrating that the beam size dependence of the tune shift is negligible. The results reveal that if the condition:

$$\frac{\gamma_s \sigma_z}{\sqrt{2}a} \gtrsim 5, \tag{104}$$

is satisfied, the approximate formula (95) or the conventional formula (4) well approximates the exact results. Meanwhile, for a nonrelativistic short bunch case that does not satisfy the

condition, the conventional formula (4) or the approximate formula (95) may overestimate the coherent tune shift, consistent with the results shown in Fig. 4.

In the context of the conductive chamber, there exists an additional factor stemming from $\bar{\Phi}^{(2)}$ that could potentially influence the tune shift. This particular contribution can be described after substituting Eq. (89) into (18), such as

$$\Delta\nu_{sp,coh}^{(2)} = -\frac{r_p N_b R^2}{2\nu_{T,0}\pi a \beta_s^2 \gamma_s^2}$$
$$\times \int_0^\infty d\bar{k}\Re\left[\frac{Ae^{-\frac{1}{2}\bar{k}^2(\gamma_s^2\sigma_z^2 - \sigma_x^2)}\bar{k}^2}{\sqrt{\bar{k}}I_0(\bar{k}a)(I_0(\bar{k}a) - A\sqrt{\bar{k}}I_0'(\bar{k}a))}\right.$$
$$\left. + \frac{Ae^{-\frac{1}{2}\bar{k}^2(\gamma_s^2\sigma_z^2 - \sigma_x^2)}\bar{k}^2}{\sqrt{\bar{k}}I_1(\bar{k}a)(I_1(\bar{k}a) - A\sqrt{\bar{k}}I_1'(\bar{k}a))}\right], \tag{105}$$

where the parameter A is given by

$$A = \sqrt{\frac{\beta_s^3\gamma_s^3\mu'}{Z_0 \mathbf{j}\sigma}}. \tag{106}$$

In the scenario of a typical conductive material, where

$$\sqrt{\frac{\beta_s^3\gamma_s^3\mu'}{Z_0\sigma(\gamma_s^2\sigma_z^2 - \sigma_x^2)^{\frac{1}{2}}}} \ll 1, \tag{107}$$

the terms proportional to A in the denominators of Eq. (105) can be disregarded. Consequently, Eq. (105) can be approximated as follows:

$$\Delta\nu_{sp,coh}^{(2)} \simeq -\frac{r_p N_b R^2}{2\nu_{T,0}\pi a \beta_s^2 \gamma_s^2} \int_0^\infty d\bar{k}\Re\left[\frac{Ae^{-\frac{1}{2}\bar{k}^2(\gamma_s^2\sigma_z^2 - \sigma_x^2)}\bar{k}^{\frac{3}{2}}}{I_0^2(\bar{k}a)} + \frac{Ae^{-\frac{1}{2}\bar{k}^2(\gamma_s^2\sigma_z^2 - \sigma_x^2)}\bar{k}^{\frac{3}{2}}}{I_1^2(\bar{k}a)}\right]$$

$$= -\frac{r_p N_b R^2}{\nu_{T,0}\pi a^3 \beta_s \gamma_s}\sqrt{\frac{\beta_s\mu'}{2Z_0\sigma\sigma_z}}\frac{2^{\frac{9}{4}}\Gamma[\frac{5}{4}]}{\left(1 - \frac{\sigma_x^2}{\gamma_s^2\sigma_z^2}\right)^{\frac{1}{4}}} - \frac{r_p N_b R^2 \Gamma[\frac{5}{4}]}{2\nu_{T,0}\pi a^3 \beta_s^2 \gamma_s^2}\sqrt{\frac{\beta_s^3\gamma_s^3\mu'}{2Z_0\sigma a}}$$

$$\times \sum_{k=1}^{\infty}\left\{\frac{\left[\frac{a^{\frac{1}{2}}2^{\frac{9}{4}}}{(\gamma_s^2\sigma_z^2 - \sigma_x^2)^{\frac{1}{4}}} - \sqrt{j_{0k}}\left(5 + \frac{2j_{0k}^2(\gamma_s^2\sigma_z^2 - \sigma_x^2)}{a^2}\right)e^{\frac{j_{0k}^2(\gamma_s^2\sigma_z^2 - \sigma_x^2)}{2a^2}}\Gamma\left[-\frac{1}{4}, \frac{j_{0k}^2(\gamma_s^2\sigma_z^2 - \sigma_x^2)}{2a^2}\right]\right]}{2J_1^2[j_{0k}]}\right.$$

$$\left. + \frac{\left[-\frac{2^{\frac{9}{4}}\sqrt{a}}{(\gamma_s^2\sigma_z^2 - \sigma_x^2)^{\frac{1}{4}}} + \sqrt{j_{1k}}\left(5 + \frac{2j_{1k}^2(\gamma_s^2\sigma_z^2 - \sigma_x^2)}{a^2}\right)e^{\frac{j_{1k}^2(\gamma_s^2\sigma_z^2 - \sigma_x^2)}{2a^2}}\Gamma\left[-\frac{1}{4}, \frac{j_{1k}^2(\gamma_s^2\sigma_z^2 - \sigma_x^2)}{2a^2}\right]\right]}{2J_0^2[j_{1k}]}\right\}. \tag{108}$$

Here, we use the following integral expressions:

$$\int_0^\infty dz \frac{e^{-\frac{(\gamma_s^2\sigma_z^2 - \sigma_x^2)}{2a^2}z^2}z^{\frac{3}{2}}}{I_0^2(z)} = \int_0^\infty dz e^{-\frac{(\gamma_s^2\sigma_z^2 - \sigma_x^2)}{2a^2}z^2}z^{\frac{3}{2}} - \sum_{k=1}^{\infty}\int_0^\infty dz \frac{4e^{-\frac{(\gamma_s^2\sigma_z^2 - \sigma_x^2)}{2a^2}z^2}z^{\frac{7}{2}}}{(z^2 + j_{0k}^2)^2 J_1^2[j_{0k}]}$$

$$= \frac{a^{\frac{5}{2}}2^{\frac{1}{4}}\Gamma[\frac{5}{4}]}{(\gamma_s^2\sigma_z^2 - \sigma_x^2)^{\frac{5}{4}}} + \sum_{k=1}^{\infty}\frac{\Gamma[\frac{5}{4}]\left(\frac{a^{\frac{1}{2}}2^{\frac{9}{4}}}{(\gamma_s^2\sigma_z^2 - \sigma_x^2)^{\frac{1}{4}}} - \sqrt{j_{0k}}\left(5 + \frac{2j_{0k}^2(\gamma_s^2\sigma_z^2 - \sigma_x^2)}{a^2}\right)e^{\frac{j_{0k}^2(\gamma_s^2\sigma_z^2 - \sigma_x^2)}{2a^2}}\Gamma\left[-\frac{1}{4}, \frac{j_{0k}^2(\gamma_s^2\sigma_z^2 - \sigma_x^2)}{2a^2}\right]\right)}{2J_1^2[j_{0k}]}, \tag{109}$$

and

$$\int_0^\infty dz \frac{e^{-\frac{(\gamma_s^2\sigma_z^2-\sigma_x^2)}{2a^2}z^2}z^{\frac{3}{2}}}{I_1^2(z)} = \int_0^\infty dz\, e^{-\frac{(\gamma_s^2\sigma_z^2-\sigma_x^2)}{2a^2}z^2}z^{-\frac{1}{2}}(4-z^2) + \sum_{k=1}^\infty \int_0^\infty dz \frac{e^{-\frac{(\gamma_s^2\sigma_z^2-\sigma_x^2)}{2a^2}z^2}z^{\frac{7}{2}}4}{(j_{1k}^2+z^2)^2 J_0^2[j_{1k}]}$$

$$= \frac{2^{\frac{1}{4}}a^{\frac{5}{2}}(-1+\frac{8(\gamma_s^2\sigma_z^2-\sigma_x^2)}{a^2})\Gamma[\frac{5}{4}]}{(\gamma_s^2\sigma_z^2-\sigma_x^2)^{\frac{5}{4}}} + \sum_{k=1}^\infty \frac{\Gamma[\frac{5}{4}]\left(-\frac{2^{\frac{9}{4}}\sqrt{a}}{(\gamma_s^2\sigma_z^2-\sigma_x^2)^{\frac{1}{4}}}+\sqrt{j_{1k}}\left(5+\frac{2j_{1k}^2(\gamma_s^2\sigma_z^2-\sigma_x^2)}{a^2}\right)e^{\frac{j_{1k}^2(\gamma_s^2\sigma_z^2-\sigma_x^2)}{2a^2}}\Gamma\left[-\frac{1}{4},\frac{j_{1k}^2(\gamma_s^2\sigma_z^2-\sigma_x^2)}{2a^2}\right]\right)}{2J_0^2[j_{1k}]},$$

$$(110)$$

through Eqs. (B1) and (B2). In these equations, $j_{mk}(= \zeta_{mk}a)$ represents the zeros of Bessel functions $J_m[x]$. It is notable that the leading-order term in Eq. (108) is naturally proportional to $1/\gamma_s$ after the cancellation between the first and second terms in Eq. (105) is performed. Similar to the calculation of $\nu_{sp,coh}^{(1)}$, this formula is expanded using the zeros of Bessel functions, which corresponds to the superposition of the image currents. The proof for the expansion formulas (B1) and (B2) with respect to the zeros of Bessel functions is given in Appendix B.

Equation (108) can be further simplified in the context of relativistic conditions, specifically when

$$\frac{\pi^2(\gamma_s^2\sigma_z^2-\sigma_x^2)}{2a^2} \gg 1, \qquad (111)$$

leading to the following expression:

$$\Delta\nu_{sp,coh}^{(2)} \simeq -\frac{r_p N_b R^2}{\nu_{T,0}\pi a^3 \beta_s \gamma_s}\sqrt{\frac{\beta_s\mu'}{2Z_0\sigma\sigma_z}}\frac{2^{\frac{1}{4}}\Gamma[\frac{5}{4}]}{\left(1-\frac{\sigma_x^2}{\gamma_s^2\sigma_z^2}\right)^{\frac{1}{4}}}, \qquad (112)$$
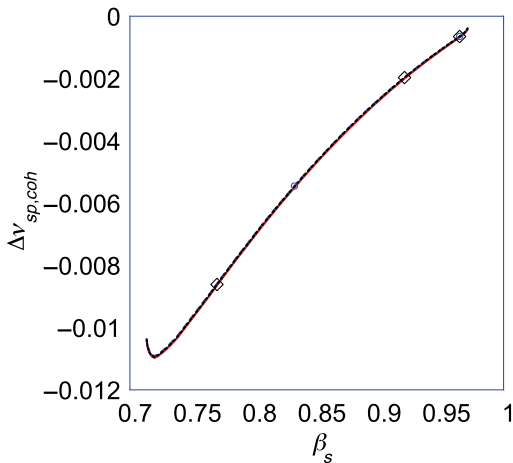

FIG. 6. Space-charge tune shifts, featuring the black dot line with "◇" and the blue dashed line with "○" representing Eqs. (4) and (93), respectively. The red solid line corresponds to the outcomes derived from Eq. (93) when considering the impact of Eq. (112).

where the expansion formulas

$$e^x\Gamma\left[-\frac{1}{4},x\right] \simeq \frac{1}{x^{\frac{5}{4}}}, \qquad (113)$$

are employed for large x. Notably, the dominant term that scales with $1/\gamma_s$ remains significant in Eq. (112), even under the relativistic condition indicated by Eq. (111).

Now, let us examine the impact of the contribution from Eq. (112) on the space-charge tune shift using the same set of parameters that led to the results in Fig. 3. Additionally, we consider a relative permeability $\mu' = 1$ and a conductivity of $\sigma = 1.35 \times 10^6$ S/m. The outcomes are illustrated in Fig. 6, where the black dot line with "◇" and the blue dashed line with "○" represent Eqs. (4) and (93), respectively.

The red solid line represents the outcomes obtained using Eq. (93), which encompasses the influence of Eq. (112). A close alignment between the red solid line and the blue dashed line with "○" is observed, indicating that the impact stemming from Eq. (112) holds little significance, when we neglect the wakefield effects from previous bunches in the accelerator [13].

It becomes apparent that the contribution arising from Eq. (112) does not carry significant weight, primarily due to the elevated conductivity σ. This implies that the Lorentz-γ_s dependency present in Eq. (112) does not hold a prominent role in determining the space-charge tune shifts, even when the material of the chamber is taken into account. In other words, the conventional formula (4) is applicable regardless of the chamber material as long as the condition (104) is satisfied.

B. Incoherent tune shift

In this section, our attention turns to the incoherent tune shift, followed by a revisit to Eq. (69). Under the approximation of $\Lambda \gg 2\sigma_x$ and assuming $r_0 = 0$, we calculate the second derivative of Eq. (69) for x after applying synthetic differential. In this particular scenario, only the term with $m = 0$ remains, leading to the following expression:

$$\frac{\partial^2 \bar{\Phi}(\rho, \varphi, \bar{z})}{\partial x^2}\bigg|_{\rho=r_0=0} = \frac{\partial^2 \bar{\Phi}_{\text{inc}}^{(1)}}{\partial x^2}\bigg|_{\rho=r_0=0} + \frac{\partial^2 \bar{\Phi}_{\text{inc}}^{(2)}}{\partial x^2}\bigg|_{\rho=r_0=0},\tag{114}$$

where

$$\frac{\partial^2 \bar{\Phi}_{\text{inc}}^{(1)}}{\partial x^2}\bigg|_{\rho=r_0=0} = -\frac{cZ_0}{\pi^2}\frac{eN_b}{2a^2}\sum_{j=1}^{\infty}\frac{\xi_{0,j}^2 e^{-\frac{1}{2}\xi_{0,j}^2 \sigma_x^2}}{[J_0'(\xi_{0,j}a)]^2}\int_0^{\infty} d\bar{k}\frac{e^{-\frac{1}{2}\bar{k}^2 \bar{\sigma}_z^2}\cos[\bar{k}\,\bar{z}]}{(\bar{k}^2 + \xi_{0,j}^2)},\tag{115}$$

$$\frac{\partial^2 \bar{\Phi}_{\text{inc}}^{(2)}}{\partial x^2}\bigg|_{\rho=r_0=0} = -\Re\left\{\sqrt{\frac{\beta_s^3 \gamma_s^3 \mu'}{\mathbf{j}Z_0\sigma}}\frac{cZ_0 eN_b}{4\pi^2 a}\int_0^{\infty} d\bar{k}\frac{\bar{k}^2 e^{-\mathbf{j}\bar{k}\,\bar{z}}e^{-\frac{1}{2}\bar{k}^2(\bar{\sigma}_z^2 - \sigma_x^2)}}{\sqrt{\bar{k}}I_0(\bar{k}a)\left(I_0[a\bar{k}] - \sqrt{\frac{\beta_s^3 \gamma_s^3 \mu'}{\mathbf{j}kZ_0\sigma}}\bar{k}I_0'[a\bar{k}]\right)}\right\},\tag{116}$$

after Eqs. (73) and (86) are applied.

It is important to note that Eqs. (115) and (116) in Eq. (114), which pertain to the incoherent tune shifts, differ from Eqs. (80) and (89) in Eq. (79), respectively, as the latter deals with coherent tune shifts.

The expression for the incoherent tune shift $\Delta\nu_{sp,incoh}^{(1)}$ in the context of a perfectly conductive chamber is finally given by

$$\Delta\nu_{sp,incoh}^{(1)} = -\frac{r_p N_b R^2}{\nu_{T,0}\pi a^3 \beta_s^2 \gamma_s^2}\sum_{j=1}^{\infty}\frac{(\xi_{0,j}a)^2}{[J_0'(\xi_{0,j}a)]^2}e^{-\frac{\sigma_x^2(\xi_{0,j}a)^2}{2a^2}}\int_0^{\infty}d\bar{k}\frac{e^{-\frac{1}{2}\bar{k}^2\frac{\gamma_s^2\sigma_z^2}{a^2}}\cos\left[\bar{k}\frac{\gamma_s(z-\beta_s ct)}{a}\right]}{(\bar{k}^2 + \xi_{0,j}^2 a^2)},\tag{117}$$

after substituting (115) into (19). In this expression, we utilize Eq. (6) and the integral representation:

$$\int_0^{\infty} d\lambda\frac{e^{-\frac{\lambda^2\gamma_s^2\sigma_z^2}{2a^2}}\cos[\lambda\frac{\bar{z}}{a}]}{(\lambda^2 + \xi_{m,j}^2 a^2)} = \begin{cases} \sum_{k=0}^{\infty}\frac{(-1)^k e^{\frac{(\xi_{m,j}a)^2\gamma_s^2\sigma_z^2}{2a^2}}(\frac{\bar{z}}{a})^{2k}(\xi_{m,j}a)^{2k-1}\Gamma[\frac{1}{2}+k]\Gamma\left[\frac{1}{2}-k,\frac{(\xi_{m,j}a)^2\gamma_s^2\sigma_z^2}{2a^2}\right]}{2(2k)!}, & \text{for } \bar{z}\neq 0, \\[2em] \frac{e^{\frac{(\xi_{m,j}a)^2\gamma_s^2\sigma_z^2}{2a^2}}\pi\text{Erfc}\left[\frac{(\xi_{m,j}a)\gamma_s\sigma_z}{\sqrt{2}a}\right]}{2(\xi_{m,j}a)}, & \text{for } \bar{z}=0. \end{cases}\tag{118}$$

To examine the contribution of the direct space effect in the incoherent tune shift, we consider the limit of an infinite radius a in Eq. (117), taking into account Eqs. (91), (92), and (118). As a result, Eq. (117) is replaced by

$$\begin{aligned}\Delta\nu_{sp,incoh}^{(1)} &= -\frac{r_p N_b R^2}{2\nu_{T,0}\pi a^4 \beta_s^2 \gamma_s^2}\int_0^{\infty}dx x^3 e^{-\frac{\sigma_x^2 x^2}{2a^2}}\int_0^{\infty}d\lambda\frac{e^{-\frac{1}{2}\lambda^2\gamma_s^2\sigma_z^2}\cos[\lambda\gamma_s(z-\beta_s ct)]}{(\lambda^2 + \frac{x^2}{a^2})} \\[1em] &= -\sum_{k=0}^{\infty}\frac{r_p N_b R^2}{4\nu_{T,0}\pi\beta_s^2\gamma_s^2}\frac{(-\gamma_s^2(z-\beta_s ct)^2)^k\Gamma[\frac{1}{2}+k]}{(2k)!}\int_0^{\infty}dx x^{2k}x^2 e^{-\frac{(\sigma_x^2-\gamma_s^2\sigma_z^2)x^2}{2}}\Gamma\left[\frac{1}{2}-k,\frac{x^2\gamma_s^2\sigma_z^2}{2}\right] \\[1em] &= -\frac{r_p N_b R^2}{2\sqrt{2\pi}\nu_{T,0}\beta_s^2\gamma_s^3\sigma_z\sigma_x^2}e^{-\frac{(z-\beta_s ct)^2}{2\sigma_z^2}} + \sum_{k=0}^{\infty}\frac{r_p N_b R^2}{\sqrt{2}\nu_{T,0}\pi\beta_s^2\gamma_s^5\sigma_z^3}\frac{(-(z-\beta_s ct)^2)^k}{(2k)!}\frac{2^k\Gamma[\frac{3}{2}+k]\,_2F_1\left[1,\frac{3}{2}+k,\frac{5}{2}+k,1-\frac{\sigma_x^2}{\gamma_s^2\sigma_z^2}\right]}{\sigma_z^{2k}(3+2k)}.\end{aligned}\tag{119}$$

In the derivation, we employ the relationships:

$$\int_0^{\infty}dx x^{2k+2}e^{-\frac{(\sigma_x^2-\bar{\sigma}_z^2)x^2}{2}}\Gamma\left[\frac{1}{2}-k,\frac{x^2\bar{\sigma}_z^2}{2}\right] = \frac{2^{k+1}}{\sqrt{2}\bar{\sigma}_z^{1+2k}\sigma_x^2} - \frac{2^k(1+2k)\Gamma[\frac{3}{2}+k]\,_2F_1\left[1,\frac{3}{2}+k,\frac{5}{2}+k,1-\frac{\sigma_x^2}{\bar{\sigma}_z^2}\right]}{\sqrt{2}\bar{\sigma}_z^{3+2k}\Gamma[\frac{5}{2}+k]},\tag{120}$$

$$\sum_{k=0}^{\infty} \frac{(-\bar{z}^2)^k}{(2k)!} \Gamma\left[\frac{1}{2}+k\right] \frac{2^k}{\bar{\sigma}_z^{2k}} = e^{-\frac{\bar{z}^2}{2\bar{\sigma}_z^2}} \sqrt{\pi}. \quad (121)$$

Consequently, we determine the incoherent tune shift for relativistic beams due to the direct space-charge effect, yielding

$$\Delta\nu_{sp,incoh}^{(1)} = -\frac{R n_b N_b r_p}{2\pi\nu_{T,0}\left(\frac{n_b\sqrt{2\pi}\sigma_z}{2\pi R}\right)\beta_s^2\gamma_s^3} \frac{1}{2\sigma_x^2} e^{-\frac{(z-\beta_s ct)^2}{2\sigma_z^2}}. \quad (122)$$

This equation replicates Eq. (5) because of $B \simeq B_f$ by substituting $\beta_s ct$ in place of z. It is important to highlight

that even though Eq. (5) was originally derived with the assumption of a coasting beam, and subsequently applied to a bunched beam, the current formalism reproduces the identical result by directly considering the bunched beam from the beginning. As a result, we can clearly observe the longitudinal dependence of the tune shift, which follows a Gaussian pattern corresponding to the beam's shape.

Let us proceed by approximating Eq. (117), which already accounts for both the direct and indirect space-charge effects, particularly focusing on the scenario where $\gamma_s^2\sigma_z^2 \gg 2a^2$. This approximation yields the following expression:

$$\Delta\nu_{sp,incoh}^{(1)} = -\frac{r_p N_b R^2}{\nu_{T,0}\pi a^3\beta_s^2\gamma_s^2} \sum_{j=1}^{\infty} \frac{(\xi_{0,j}a)^2}{[J_0'(\xi_{0,j}a)]^2} e^{-\frac{\sigma_x^2(\xi_{0,j}a)^2}{2a^2}} \int_0^{\infty} d\bar{k} \frac{e^{-\frac{1}{2}\bar{k}^2\frac{\gamma_s^2\sigma_z^2}{a^2}}\cos\left[\bar{k}\frac{\gamma_s(z-\beta_s ct)}{a}\right]}{(\bar{k}^2 + \xi_{0,j}^2 a^2)}$$

$$\simeq -\frac{r_p(n_b N_b)R}{2\pi\nu_{T,0}\left(\frac{n_b\sqrt{2\pi}\sigma_z}{2\pi R}\right)\beta_s^2\gamma_s^3} \frac{e^{-\frac{(z-\beta_s ct)^2}{4\sigma_z^2}}}{a^2} \sum_{j=1}^{\infty} \frac{e^{-\frac{\sigma_x^2(\xi_{0,j}a)^2}{2a^2}}}{[J_0'(\xi_{0,j}a)]^2}, \quad (123)$$

which is proportional to $1/\beta_s^2\gamma_s^3$. In the above derivation, we utilize the relationship

$$\int_0^{\infty} d\bar{k} e^{-\frac{1}{2}\bar{k}^2\frac{\gamma_s^2\sigma_z^2}{a^2}}\cos\left[\bar{k}\frac{\gamma_s(z-\beta_s ct)}{a}\right] = \frac{e^{-\frac{(z-\beta_s ct)^2}{4\sigma_z^2}}\sqrt{\pi}a}{\sqrt{2}\gamma_s\sigma_z}. \quad (124)$$

Equation (123) becomes infinite for infinitesimal σ_x, consistent with the result obtained in the conventional manner at the end of Sec. II B and in formula (5).

Currently, let us center our attention on the approximate outcome derived solely from Eq. (123), specifically addressing a relativistic longer pulse beam as an illustrative example. In essence, this result will be juxtaposed with

Eq. (5), wherein only the direct space-charge effect comes into play.

The left panel of Fig. 7 illustrates the computed results by Eqs. (5) (green dashed) and (123) (red solid) under the same conditions used for generating the outcomes in Fig. 3. The red solid lines in the middle and right panels depict the transverse root mean square beam size and $\gamma_s\sigma_z/\sqrt{2}$ during the ramping time, respectively. The black dot lines in the panels refer to the chamber radius a for reference. Since the right panel demonstrates $\gamma_s\sigma_z/\sqrt{2} \gg a$, the formula (123) is validated in the present example. It is worth noting that there is a numerically significant agreement between Eqs. (5) and (123) in the left panel when taking into account the provided transverse beam size shown in the middle panel.
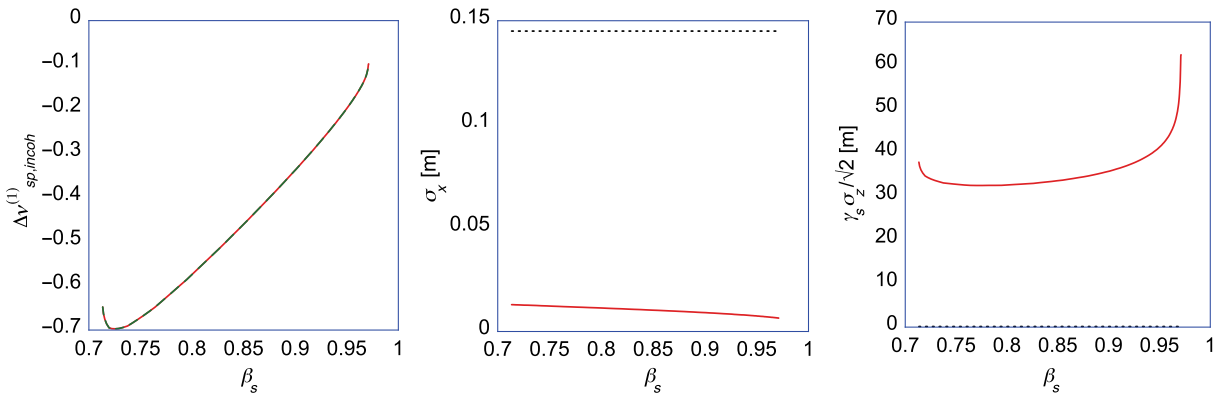

FIG. 7. Incoherent tune shifts (left), where the green dashed and red solid lines represent Eqs. (5) (conventional) and (123) (present formula), respectively. The transverse root mean square beam size (middle) and $\gamma_s\sigma_z/\sqrt{2}$ (right) are denoted by the red lines, where the black dot line refers to the chamber radius a for reference.
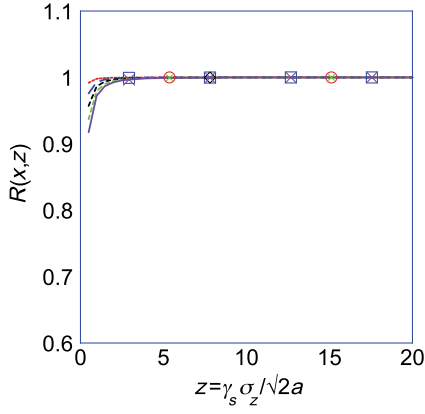
FIG. 8. The variation of function $R(x, z)$ along z. The lines in red with "○", blue dashed with "□", black dot with "◇", green dot with "×", and purple solid with "×" correspond to the cases of $x(= \sigma_x/\sqrt{2}a) = 0.028$, 0.056, 0.085, 0.113, and 0.141, respectively.

From a purely mathematical perspective, Eq. (123) suggests that the chamber could potentially affect the incoherent tune shift when the beam size is comparable to the chamber radius. However, the beam size must be significantly smaller than the chamber radius to render the Gaussian tail negligible, as discussed earlier. Consequently, when dealing with a Gaussian beam for a relativistic or longer pulse beam, the contribution from the indirect space effect generally becomes negligible in the incoherent space tune shift for a cylindrical chamber.

On the other hand, the relativistic or coasting beam approximation may lead to deviations of the conventional results from the rigorous ones for nonrelativistic shorter pulse beams. Hence, let us now calculate the ratio of Eqs. (117) with $z = \beta_s ct$ to Eq. (123), defined as

$$
R\left(x = \frac{\sigma_x}{\sqrt{2}a}, z = \frac{\gamma_s \sigma_z}{\sqrt{2}a}\right)
$$

$$
= \sqrt{\pi} z \frac{\sum_{j=1}^{\infty} \frac{(\xi_{0,j}a)e^{-(x^2-z^2)(\xi_{0,j}a)^2}}{(J_0'(\xi_{0,j}a))^2} \mathrm{Erfc}[(\xi_{0,j}a)z]}{\sum_{j=1}^{\infty} \frac{e^{-(\xi_{0,j}a)^2 x^2}}{[J_0'(\xi_{0,j}a)]^2}}, \quad (125)
$$

and investigate its behavior along z for fixed x, following a similar approach as in the coherent case. Figure 8 shows the results for the same set of parameters in Fig. 5, where the lines in red with "○", blue dashed with "□", black dot with "◇", green dot with "×", and purple solid with "×" correspond to the cases of $x(= \sigma_x/\sqrt{2}a) = 0.028$, 0.056, 0.085, 0.113, and 0.141, respectively.

Similar to the coherent tune shift, the condition (104) acts as a reliable criterion for utilizing both the conventional formula (5) and the approximate one (123) to judge whether they well approximate the exact formula (117). For a nonrelativistic short bunch case that does not satisfy the condition, the conventional formula (5) or the approximate formula (123) may slightly overestimate the incoherent tune shift by around 10% for a beam with a broader transverse beam size, such as $\sigma_x/\sqrt{2}a = 0.141$, due to the effect of the chamber boundary.

Overall, the comparison between Figs. 5 and 8 illustrates that the influence of $\gamma_s \sigma_z$ on the deviation of the conventional formula (5) from the rigorous results in (117) is relatively minor compared to the case of the coherent tune shift. However, the dependence on the transverse beam size is more pronounced in the incoherent tune shift.

The contribution arising from the second term of Eq. (114) attributed to the chamber material, as given by Eq. (116), can be approximated in the following manner:

$$
\frac{\partial^2 \bar{\Phi}_{\mathrm{inc}}^{(2)}}{\partial x^2}\bigg|_{\rho=r_0=0} = -\Re \left\{ \sqrt{\frac{\beta_s^3 \gamma_s^3 \mu'}{\mathbf{j} Z_0 \sigma}} \frac{c Z_0 e N_b}{4\pi^2 a^2 a^{\frac{3}{2}}} \int_0^{\infty} d\bar{k}a \frac{\bar{k}^2 a^2 e^{-\mathbf{j}\bar{k}a\frac{\bar{z}}{a}} e^{-\frac{(\bar{\sigma}_z^2 - \sigma_x^2)}{2a^2}\bar{k}^2 a^2}}{\sqrt{\bar{k}a} I_0(\bar{k}a)\left(I_0[a\bar{k}] - \sqrt{\frac{\beta_s^3 \gamma_s^3 \mu'}{\mathbf{j} k Z_0 \sigma}}\bar{k} I_0'[a\bar{k}]\right)} \right\}
$$

$$
\simeq -\Re \left\{ \sum_{n=0}^{\infty} \sqrt{\frac{\beta_s^3 \gamma_s^3 \mu'}{\mathbf{j} Z_0 \sigma}} \frac{c Z_0 e N_b (-\mathbf{j}\frac{\bar{z}}{a})^n}{4\pi^2 a^2 a^{\frac{3}{2}} n!} \int_0^{\infty} d(\bar{k}a) \frac{(\bar{k}a)^{2+n} e^{-\frac{(\bar{\sigma}_z^2 - \sigma_x^2)}{2a^2}\bar{k}^2 a^2}}{\sqrt{\bar{k}a} I_0^2(\bar{k}a)} \right\}
$$

$$
= -\Re \left\{ \sqrt{\frac{\beta_s^3 \gamma_s^3 \mu'}{\mathbf{j} Z_0 \sigma}} \frac{c Z_0 e N_b 2^{\frac{1}{4}}}{4\pi^2 a (\bar{\sigma}_z^2 - \sigma_x^2)^{\frac{5}{4}}} \sum_{n=0}^{\infty} \frac{\left(-\mathbf{j}\frac{\sqrt{2}\bar{z}}{\sqrt{(\bar{\sigma}_z^2 - \sigma_x^2)}}\right)^n \Gamma[\frac{5}{4} + \frac{n}{2}]}{n!} \right\} + \Re \left\{ \sqrt{\frac{\beta_s^3 \gamma_s^3 \mu'}{\mathbf{j} Z_0 \sigma}} \frac{c Z_0 e N_b}{8\pi^2 a^2 a^{\frac{3}{2}}} \sum_{n=0}^{\infty} \frac{(-\mathbf{j}\frac{\bar{z}}{a})^n \Gamma[\frac{5}{4} + \frac{n}{2}]}{n!} \right.
$$

$$
\times \sum_{k=1}^{\infty} \frac{\left[-\frac{2^{\frac{9}{4}+\frac{n}{2}} a^{\frac{1}{2}+n}}{(\bar{\sigma}_z^2 - \sigma_x^2)^{\frac{1}{4}+\frac{n}{2}}} + j_{0k}^{\frac{1}{2}+n}\left(5 + 2n + \frac{2j_{0k}^2(\bar{\sigma}_z^2 - \sigma_x^2)}{a^2}\right) e^{\frac{j_{0k}^2(\bar{\sigma}_z^2 - \sigma_x^2)}{2a^2}} \Gamma\left[-\frac{1}{4} - \frac{n}{2}, \frac{j_{0k}^2(\bar{\sigma}_z^2 - \sigma_x^2)}{2a^2}\right]\right]}{J_1^2[j_{0k}]} \right\}. \quad (126)
$$

This is obtained by utilizing the following relation:

$$
\int_0^\infty dz \frac{z^{n+2} e^{-z^2 \frac{(\bar\sigma_z^2 - \sigma_x^2)}{2a^2}}}{z^{\frac12} I_0^2(z)} = \int_0^\infty dz z^{n+\frac32} e^{-z^2 \frac{(\bar\sigma_z^2 - \sigma_x^2)}{2a^2}} - \sum_{k=1}^\infty \int_0^\infty dz \frac{4 z^{n+\frac72} e^{-\frac12 z^2 \frac{(\bar\sigma_z^2 - \sigma_x^2)}{a^2}}}{(z^2 + j_{0k}^2)^2 J_1^2[j_{0k}]}
$$

$$
= \frac{2^{\frac14+\frac{n}{2}} a^{\frac52+n} \Gamma[\frac54 + \frac{n}{2}]}{(\bar\sigma_z^2 - \sigma_x^2)^{\frac54+\frac{n}{2}}} - \sum_{k=1}^\infty \frac{\Gamma[\frac54 + \frac{n}{2}]\left[-\frac{2^{\frac94+\frac{n}{2}} a^{\frac12+n}}{(\bar\sigma_z^2 - \sigma_x^2)^{\frac14+\frac{n}{2}}} + j_{0k}^{\frac12+n}\left(5 + 2n + \frac{2 j_{0k}^2(\bar\sigma_z^2-\sigma_x^2)}{a^2}\right) e^{\frac{j_{0k}^2(\bar\sigma_z^2-\sigma_x^2)}{2a^2}} \Gamma\left[-\frac14 - \frac{n}{2}, \frac{j_{0k}^2(\bar\sigma_z^2-\sigma_x^2)}{2a^2}\right]\right]}{2 J_1^2[j_{0k}]},
$$

(127)

alongside Eq. (B1). Notably, it is evident that Eq. (127) reproduces (109) when substituting $n = 0$ into it.

In the case of

$$
\frac{\pi^2(\bar\sigma_z^2 - \sigma_x^2)}{2a^2} \gg 1,
$$

(128)

since we can apply for the expansion formulas:

$$
e^x \Gamma\left[-\frac14 - \frac{n}{2}, x\right] \simeq \frac14 x^{-\frac94 - \frac{n}{2}}(-5 - 2n + 4x),
$$

(129)

for $x \gg 1$, consistent with Eq. (113) in the case of $n = 0$, Eq. (126) is approximated as

$$
\left.\frac{\partial^2 \bar\Phi_{\text{inc}}^{(2)}}{\partial x^2}\right|_{\rho=r_0=0} = -\Re\left\{\sqrt{\frac{\beta_s^3 \gamma_s^3 \mu'}{\mathbf{j} Z_0 \sigma}} \frac{c Z_0 e N_b 2^{\frac14}}{4\pi^2 a (\bar\sigma_z^2 - \sigma_x^2)^{\frac54}} \sum_{n=0}^\infty \frac{\left(-\mathbf{j} \frac{\sqrt{2}\bar z}{\sqrt{(\bar\sigma_z^2 - \sigma_x^2)}}\right)^n \Gamma[\frac54 + \frac{n}{2}]}{n!}\right\}
$$

$$
- \Re\left\{\sqrt{\frac{\beta_s^3 \gamma_s^3 \mu'}{\mathbf{j} Z_0 \sigma}} \frac{c Z_0 e N_b 2^{\frac14} a}{16\pi^2 (\bar\sigma_z^2 - \sigma_x^2)^{\frac94}} \sum_{n=0}^\infty \frac{\left(-\mathbf{j} \frac{\sqrt{2}\bar z}{\sqrt{(\bar\sigma_z^2 - \sigma_x^2)}}\right)^n (5 + 2n) \Gamma[\frac94 + \frac{n}{2}]}{n!}\right\},
$$

(130)

where we use

$$
\sum_{k=1}^\infty \frac{1}{j_{0k}^4 J_1^2[j_{0k}]} = \frac18,
$$

(131)

obtained by after taking a limit of z to zero in Eq. (B1).

After summing up n in Eq. (130), Eq. (130) is equal to

$$
\left.\frac{\partial^2 \bar\Phi_{\text{inc}}^{(2)}}{\partial x^2}\right|_{\rho=r_0=0} = -\sqrt{\frac{\beta_s^3 \gamma_s^3 \mu'}{2 Z_0 \sigma}} \frac{c Z_0 e N_b 2^{\frac14} \left(\Gamma[\frac14]\,_1F_1\left[\frac54, \frac12, -\frac{\bar z^2}{2(\bar\sigma_z^2 - \sigma_x^2)}\right] - \frac{3\sqrt{2}\bar z}{\sqrt{(\bar\sigma_z^2 - \sigma_x^2)}} \Gamma[\frac34]\,_1F_1\left[\frac74, \frac32, -\frac{\bar z^2}{2(\bar\sigma_z^2 - \sigma_x^2)}\right]\right)}{16\pi^2 a (\bar\sigma_z^2 - \sigma_x^2)^{\frac54}}
$$

$$
- \sqrt{\frac{\beta_s^3 \gamma_s^3 \mu'}{2 Z_0 \sigma}} \frac{c Z_0 e N_b 2^{\frac14} a}{512\pi^2 (\bar\sigma_z^2 - \sigma_x^2)^{\frac94}} \left(50\Gamma\left[\frac14\right]\,_1F_1\left[\frac94, \frac12, -\frac{\bar z^2}{2(\bar\sigma_z^2 - \sigma_x^2)}\right] - \frac{90\bar z^2}{(\bar\sigma_z^2 - \sigma_x^2)} \Gamma\left[\frac14\right]\,_1F_1\left[\frac{13}{4}, \frac32, -\frac{\bar z^2}{2(\bar\sigma_z^2 - \sigma_x^2)}\right]\right.
$$

$$
\left. - \frac{84\sqrt{2}\bar z}{\sqrt{(\bar\sigma_z^2 - \sigma_x^2)}} \Gamma\left[\frac34\right]\,_1F_1\left[\frac{11}{4}, \frac12, -\frac{\bar z^2}{2(\bar\sigma_z^2 - \sigma_x^2)}\right] - \frac{210\sqrt{2}\bar z}{\sqrt{(\bar\sigma_z^2 - \sigma_x^2)}} \Gamma\left[\frac34\right]\,_1F_1\left[\frac{11}{4}, \frac32, -\frac{\bar z^2}{2(\bar\sigma_z^2 - \sigma_x^2)}\right]\right),
$$

(132)

where we use

$$
\sum_{n=0}^\infty \frac{(-\mathbf{j}a)^n \Gamma[\frac54 + \frac{n}{2}]}{n!} = \frac14 \left(\Gamma\left[\frac14\right]\,_1F_1\left[\frac54, \frac12, -\frac{a^2}{4}\right] - \mathbf{j} 3a \Gamma\left[\frac34\right]\,_1F_1\left[\frac74, \frac32, -\frac{a^2}{4}\right]\right),
$$

(133)

$$\sum_{n=0}^{\infty} \frac{(5+2n)\Gamma[\frac{9}{4}+\frac{n}{2}](-\mathbf{j}a)^n}{n!} = \frac{1}{32}\left(50\Gamma\left[\frac{1}{4}\right]{}_1F_1\left[\frac{9}{4},\frac{1}{2},-\frac{a^2}{4}\right] - 45a^2\Gamma\left[\frac{1}{4}\right]{}_1F_1\left[\frac{13}{4},\frac{3}{2},-\frac{a^2}{4}\right]\right.$$
$$\left. - 84\mathbf{j}a\Gamma\left[\frac{3}{4}\right]{}_1F_1\left[\frac{11}{4},\frac{1}{2},-\frac{a^2}{4}\right] - 210\mathbf{j}a\Gamma\left[\frac{3}{4}\right]{}_1F_1\left[\frac{11}{4},\frac{3}{2},-\frac{a^2}{4}\right]\right), \tag{134}$$

and $_1F_1[a,b,z]$ represents Kummer's confluent hypergeometric function [20,24].

Finally, the correction term $\Delta\nu_{sp,incoh}^{(2)}$ owing to the conductive chamber material is described as

$$\Delta\nu_{sp,incoh}^{(2)} = -\frac{2^{\frac{1}{4}}R^2 r_p N_b}{8\pi a\nu_{T,0}\beta_s\gamma_s^3\sigma_z^2(1-\frac{\sigma_x^2}{\sigma_z^2\gamma_s^2})^{\frac{5}{4}}}\sqrt{\frac{\beta_s\mu'}{2Z_0\sigma\sigma_z}}$$

$$\times\left(\Gamma\left[\frac{1}{4}\right]{}_1F_1\left[\frac{5}{4},\frac{1}{2},-\frac{(z-\beta_sct)^2}{2\left(\sigma_z^2-\frac{\sigma_x^2}{\gamma_s^2}\right)}\right] - \frac{6(z-\beta_sct)\Gamma[\frac{3}{4}]{}_1F_1\left[\frac{7}{4},\frac{3}{2},-\frac{(z-\beta_sct)^2}{2\left(\sigma_z^2-\frac{\sigma_x^2}{\gamma_s^2}\right)}\right]}{\sqrt{2\left(\sigma_z^2-\frac{\sigma_x^2}{\gamma_s^2}\right)}}\right) + O\left(\frac{1}{\gamma_s^5}\right), \tag{135}$$

for relativistic or longer bunched beams, after substituting Eq. (132) into (19). Differently from Eq. (112) in the coherent tune shift case, Eq. (135) is proportional to $1/\gamma_s^3$ rather than $1/\gamma_s$. The longitudinal distribution of correction term $\Delta\nu_{sp,incoh}^{(2)}$ is characterized by the function:

$$f(x) = \Gamma\left[\frac{1}{4}\right]{}_1F_1\left[\frac{5}{4},\frac{1}{2},-x^2\right] - 6\Gamma\left[\frac{3}{4}\right]x\,{}_1F_1\left[\frac{7}{4},\frac{3}{2},-x^2\right], \tag{136}$$

which is shown in Fig. 9 whose longitudinal shape is asymmetric owing to the resistive wall effect.

Finally, let us perform a quantitative assessment of the impact due to the chamber material on the incoherent space-charge tune shift. Figure 10 presents a comparison between Eqs. (5) and (123) without the inclusion of Eq. (135), as well as th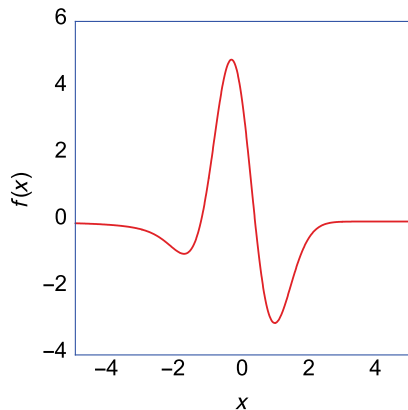e case when Eq. (135) is considered alongside (123). The red dashed "○", and black solid "◇" lines correspond to formula (123) without and with correction term (135), respectively. The green dot "△" line denotes the result by Eq. (5) for reference. This analysis is carried out under the same conditions used to produce the results in Fig. 7, and the utilization of Eq. (135) is justified since Eq. (128) is satisfied, as evidenced by the outcomes in the middle and right panels of Fig. 7. It is evident that the red dashed "○", black solid "◇", and green dot "△" lines bear a strong resemblance to each other. This observation underscores that the material properties have minimal influence on the incoherent tune shift.
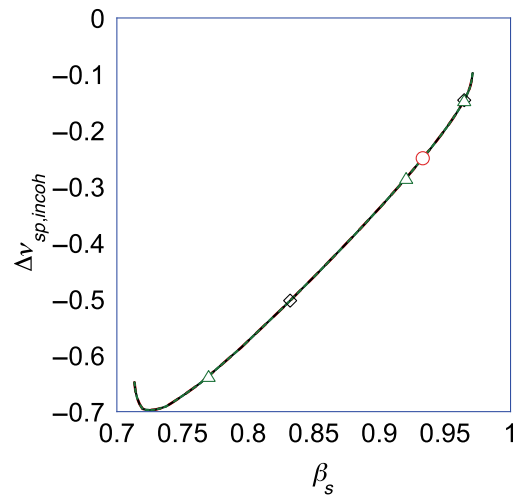

FIG. 9. Longitudinal distribution of function $f(x)$.

FIG. 10. Incoherent tune shifts: the green dot "△", the red dashed "○", and the black solid "◇" lines represent Eq. (5), Eq. (123) without Eq. (135), and Eq. (123) combined with Eq. (135), respectively.

IV. SUMMARY

The formulations used in previous studies to describe the tune shifts for a relativistic bunched beam were constructed based on the assumption of mirror currents for a coasting beam to address the chamber wall effects and then extended to the case in a somewhat intuitive manner by introducing the bunching factor. The validity of this conventional formalism has to be established more rigorously. In this paper, by employing the formalism of the Green function, which accounts for the boundary conditions and addresses the characteristics of pulsed beams, we have derived expressions for the coherent [Eq. (93) with Eq. (112)] and incoherent tune shifts [Eq. (117) with Eq. (135)] resulting from the passage of an axisymmetric bunched Gaussian beam with a wider range of transverse and longitudinal beam sizes through a cylindrical conductive chamber.

Although the comprehensive formula involving Lorentz-β, -γ dependence is intricate in general circumstances, particularly in scenarios involving relativistic beams, both the incoherent and coherent tune shifts adhere to the typical Lorentz-β, -γ dependence of $1/\beta_s^2\gamma_s^3$, provided we disregard the adiabatic damping impact on beam size.

In the case of the coherent tune shift, the rigorous results converge toward Zötter's formula (4) as Lorentz-γ increases, considering an infinitesimal transverse beam size. This convergence is attributed to the presence of the factor $\gamma_s\sigma_z$ in the rigorous formula (93), even though formula (4) was derived under the assumption of a coasting beam. It is important to emphasize that the condition (104) serves as a reliable criterion for determining the suitability of Zötter's formula (4) in describing the coherent tune shift. Otherwise, the conventional formula may overestimate the coherent tune shift in nonrelativistic shorter bunch cases. Additionally, in this investigation, we directly confirm that the direct space-charge effect cannot contribute to the coherent tune shift when a beam passes through a cylindrical chamber.

On the contrary, the incoherent tune shift is primarily governed by the direct space-charge effect when considering a Gaussian beam within a cylindrical chamber, as illustrated by formula (5). This is due to the necessity for its transverse root mean square size to be considerably smaller than the chamber radius. However, the transverse beam size could moderately influence the conventional formula (5) for nonrelativistic shorter bunch cases, in contrast to its impact on the coherent tune shift, as observed in the comparison between Figs. 5 and 8. It is worth noting that the condition (104) also serves as a reliable criterion for applying the conventional formula (5) to evaluate the incoherent tune shift for a given pulsed beam.

In order to validate the soundness of the current methodologies, we replicate the earlier findings achieved through the Green's function, with no boundary conditions imposed. This replication is carried out by considering an infinitely large chamber radius, serving as a form of consistency assessment in relation to the prior result. Furthermore, we successfully reproduce the scalar potential obtained by introducing the mirror current for the coasting beam through the integration of precise results for a pulsed beam in the longitudinal direction.

One advantage of using the Green's function formalism is its ability to consider the impact of chamber material on the tune shifts. When a bunched beam travels through a chamber with conductive material, this substance can introduce specific Lorentz-γ dependencies. For instance, it may lead to an inverse proportionality of Lorentz-γ for the coherent tune shift. Additionally, the chamber material has the potential to influence the incoherent tune shift along the longitudinal direction due to the resistive-wall effect.

However, from a quantitative standpoint, these material-induced effects do not significantly alter both the coherent and incoherent tune shifts, primarily due to the substantial conductivity of the material, unless we consider the wake-field effects created by previous bunches.

ACKNOWLEDGMENT

APPENDIX A: DERIVATION OF FORMULA (10)

In this Appendix, we provide the derivation of formula (10) presented in the main text. To address the Poisson equation (8), we partition the beam density into several concentric shells. For each shell determined by the parameter τ, we introduce a Poisson equation as follows:

$$\triangle\bar{\Phi}(x,y,\bar{z};\tau) = -\frac{eN_bcZ_0}{(2\pi)^{3/2}\sigma_x\sigma_y\bar{\sigma}_z}2\tau e^{-\frac{\tau^2}{2}}$$
$$\times\delta\left(\left(\frac{x^2}{a}+\frac{y^2}{b}+\frac{\bar{z}^2}{c}-1\right)\tau^2\right). \quad (A1)$$

Here, $a = \tau^2\sigma_x^2$, $b = \tau^2\sigma_y^2$, and $c = \tau^2\bar{\sigma}_z^2$ with the assumption that $a < b < c$.

In the end, the solution to Eq. (8) can be obtained by integrating the solution of Eq. (A1) with respect to the variable τ over the range from zero to infinity.

By introducing ellipsoidal coordinates (ξ, η, ζ), defined as the three solutions of the cubic equation [26,27]:

$$\frac{x^2}{a-\mu}+\frac{y^2}{b-\mu}+\frac{\bar{z}^2}{c-\mu} = 1, \quad (A2)$$

where μ is chosen to satisfy the conditions ($-\infty < \xi < a < \eta < b < \zeta < c$), the function $\bar{\Phi}(x,y,\bar{z};\tau)$ can be expressed as a function of only ξ. Thus, Eq. (A1) can be simplified to

$$\frac{4\sqrt{Q(\xi)}}{(\eta-\xi)(\zeta-\xi)}\frac{\partial}{\partial\xi}\left[\sqrt{Q(\xi)}\frac{\partial\bar{\Phi}(\xi;\tau)}{\partial\xi}\right]$$
$$=-\frac{eN_b cZ_0}{(2\pi)^{3/2}\sigma_x\sigma_y\bar{\sigma}_z}2\tau e^{-\frac{\tau^2}{2}}\frac{abc}{\tau^2(\zeta-\xi)(\eta-\xi)}\delta(\xi), \quad \text{(A3)}$$

where $Q(\xi)=(a-\xi)(b-\xi)(c-\xi)$.

The solution to Eq. (A3) takes the form:

$$\bar{\Phi}(\xi;\tau)=\int_{-\infty}^{\xi}\frac{\hat{\beta}(\xi')}{\sqrt{(a-\xi')(b-\xi')(c-\xi')}}d\xi', \quad \text{(A4)}$$

where

$$\hat{\beta}(\xi)=-\frac{eN_b cZ_0}{2(2\pi)^{3/2}}\tau^2 e^{-\frac{\tau^2}{2}}\Theta(\xi)+c_1. \quad \text{(A5)}$$

Here, c_1 is an arbitrary constant and $\Theta(\xi)$ represents the step function. The regions where $\xi<0$ and $\xi\geq0$ correspond to the areas outside and inside the shell, respectively.

In order to determine the constant c_1, let us examine the asymptotic behavior of $\bar{\Phi}(\xi;\tau)$ as ξ approaches negative infinity. This behavior is given by

$$\bar{\Phi}(\xi;\tau)\to\frac{2c_1}{\sqrt{-\xi}}=\frac{2c_1}{\sqrt{x^2+y^2+\bar{z}^2}}=\frac{Q_\tau}{4\pi\epsilon_0\sqrt{x^2+y^2+\bar{z}^2}}, \quad \text{(A6)}$$

where Q_τ is the total charge on the shell, and $\epsilon_0=1/cZ_0$ represents the vacuum's dielectric constant. In the given expression, the parameter ξ is expressed in relation to the original Cartesian coordinates $x,y,\bar{z}$ with reference to Eq. (A2). This is based on the understanding that the potential $\bar{\Phi}(\xi;\tau)$ approaches $Q_\tau/(4\pi\epsilon_0\sqrt{x^2+y^2+\bar{z}^2})$ as the magnitude of $\sqrt{x^2+y^2+\bar{z}^2}$ becomes large.

Meanwhile, the calculation of the total charge on the shell Q_τ proceeds as follows:

$$Q_\tau=\int_{-\infty}^{a}d\xi\int_{a}^{b}d\eta\int_{b}^{c}d\zeta\frac{eN_b}{(2\pi)^{3/2}}\frac{2e^{-\frac{\tau^2}{2}}\tau^5\sigma_x\sigma_y\bar{\sigma}_z}{(\zeta-\xi)(\eta-\xi)}\delta(\xi)$$
$$\times\frac{(\xi-\eta)(\eta-\zeta)(\zeta-\xi)}{\sqrt{-Q(\xi)Q(\eta)Q(\zeta)}}$$
$$=\frac{8eN_b\tau^2 e^{-\frac{\tau^2}{2}}}{(2\pi)^{3/2}}\left[-K\left(\sqrt{\frac{\sigma_y^2-\sigma_x^2}{\sigma_z^2-\sigma_x^2}}\right)K\left(\sqrt{\frac{\sigma_z^2-\sigma_y^2}{\sigma_z^2-\sigma_x^2}}\right)\right.$$
$$+K\left(\sqrt{\frac{\sigma_y^2-\sigma_x^2}{\sigma_z^2-\sigma_x^2}}\right)E\left(\sqrt{\frac{\sigma_z^2-\sigma_y^2}{\sigma_z^2-\sigma_x^2}}\right)$$
$$\left.+E\left(\sqrt{\frac{\sigma_y^2-\sigma_x^2}{\sigma_z^2-\sigma_x^2}}\right)K\left(\sqrt{\frac{\sigma_z^2-\sigma_y^2}{\sigma_z^2-\sigma_x^2}}\right)\right]$$
$$=\frac{4\pi eN_b}{(2\pi)^{3/2}}\tau^2 e^{-\frac{\tau^2}{2}}, \quad \text{(A7)}$$

where the recognition of the right-hand side of the Poisson equation [Eq. (A3)] is used. During the derivation, we observe that the volume element in ellipsoidal coordinates takes the form:

$$dxdyd\bar{z}=\frac{(\eta-\xi)(\zeta-\xi)(\zeta-\eta)}{8\sqrt{Q(\xi)[-Q(\eta)]Q(\zeta)}}d\xi d\eta d\zeta, \quad \text{(A8)}$$

and we also utilize Legendre's relation for the complete elliptic integral of the first kind, denoted as $K[m]$, and the second kind, denoted as $E[m]$, as stated in Refs. [20,23]:

$$E(m)K(\sqrt{1-m^2})+E(\sqrt{1-m^2})K(m)$$
$$-K(m)K(\sqrt{1-m^2})=\frac{\pi}{2}. \quad \text{(A9)}$$

Upon substituting Eq. (A7) into Eq. (A6), the coefficient c_1 is ultimately found to be

$$c_1=\frac{eN_b}{2(2\pi)^{3/2}\epsilon_0}\tau^2 e^{-\frac{\tau^2}{2}}. \quad \text{(A10)}$$

The solution to the original Poisson equation, Eq. (8), can be expressed as

$$\bar{\Phi}(\xi)=\int_{0}^{\infty}d\tau\tau^2 e^{-\frac{\tau^2}{2}}\int_{-\infty}^{\xi(\tau)}d\xi'\frac{\beta_0(\xi')}{\sqrt{(a-\xi')(b-\xi')(c-\xi')}}, \quad \text{(A11)}$$

by integrating $\bar{\Phi}(\xi;\tau)$ over τ after combining Eqs. (A4), (A5), and (A10). Here,

$$\hat{\beta}_0(\xi)=-\frac{eN_b}{2(2\pi)^{3/2}\epsilon_0}(\Theta(\xi)-1). \quad \text{(A12)}$$

Let us introduce a new parameter, $\xi_0(\tau)$, defined as

$$\xi(\tau)=\tau^2\xi_0(\tau), \quad \text{(A13)}$$

to enable a partial integration of Eq. (A11) with respect to τ. This leads to the following expression:

$$\bar{\Phi}(x,y,z)=\int_{0}^{\infty}d\tau\tau e^{-\frac{\tau^2}{2}}$$
$$\times\int_{-\infty}^{\xi_0(\tau)}d\xi''\frac{\beta_0(\xi'')}{\sqrt{(\sigma_x^2-\xi'')(\sigma_y^2-\xi'')(\bar{\sigma}_z^2-\xi'')}}$$
$$=-e^{-\frac{\tau^2}{2}}\int_{-\infty}^{\xi_0(\tau)}d\xi''\frac{\beta_0(\xi'')}{\sqrt{(\sigma_x^2-\xi'')(\sigma_y^2-\xi'')(\bar{\sigma}_z^2-\xi'')}}\Bigg|_{0}^{\infty}$$
$$+\int_{0}^{\infty}e^{-\frac{\tau^2}{2}}\frac{\beta_0(\xi_0)}{\sqrt{(\sigma_x^2-\xi_0)(\sigma_y^2-\xi_0)(\bar{\sigma}_z^2-\xi_0)}}\frac{d\xi_0}{d\tau}d\tau. \quad \text{(A14)}$$

Given that the parameter $\xi_0(\tau)$ adheres to the condition:

$$\frac{x^2}{\sigma_x^2 - \xi_0(\tau)} + \frac{y^2}{\sigma_y^2 - \xi_0(\tau)} + \frac{\bar{z}^2}{\bar{\sigma}_z^2 - \xi_0(\tau)} = \tau^2, \quad \text{(A15)}$$

we observe that $\xi_0(\tau)$ approaches σ_x^2 as τ tends to infinity, and $\xi_0(\tau)$ tends toward negative infinity as τ approaches zero. This implies that the first term of Eq. (A14) must evaluate to zero.

By amalgamating Eqs. (A12) and (A15) prior to the transformation of τ into ξ_0, the scalar potential $\bar{\Phi}(x, y, \bar{z})$ in the rest frame can ultimately be expressed as formula (10).

APPENDIX B: DERIVATION OF FORMULAS RELATED TO BESSEL FUNCTIONS

The modified Bessel functions $I_m[x]$ exhibit the following relationships:

$$\frac{1}{z^2 I_0^2(z)} = \frac{1}{z^2} - \sum_{k=1}^{\infty} \frac{4}{(z^2 + j_{0k}^2)^2 J_1^2[j_{0k}]}, \quad \text{(B1)}$$

and

$$\frac{1}{z^2 I_1^2(z)} = \frac{(4 - z^2)}{z^4} + \sum_{k=1}^{\infty} \frac{4}{(j_{1k}^2 + z^2)^2 J_0^2[j_{1k}]}. \quad \text{(B2)}$$

Here, $j_{mk}(= \zeta_{mk}a)$ represents the zeros of Bessel functions $J_m[x]$.

The aforementioned equations can be demonstrated through the following method. Let us consider the loop integral in the following form [28]:
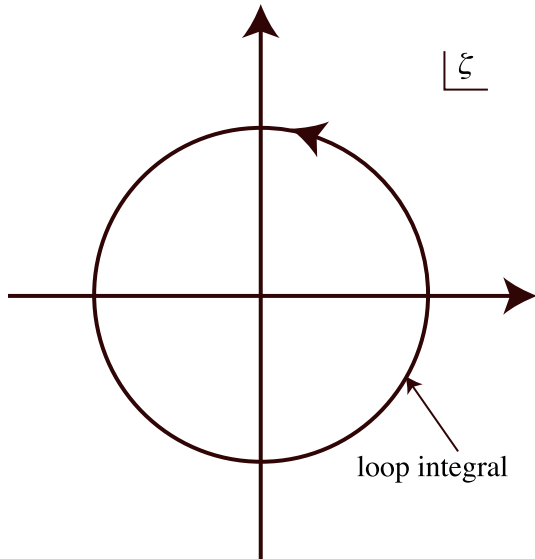

FIG. 11. The path of integration in Eq. (B3) and in order to prove Eqs. (B1), (B2), (B6), and (B7).

$$Q_m = \frac{1}{2\pi \mathbf{j}} \oint d\zeta \frac{1}{(\zeta^2 - z^2)\zeta J_m^2(\zeta)}, \quad \text{(B3)}$$

on the complex plane, where $\mathbf{j}$ represents the imaginary unit. The computation of Eq. (B3) can be carried out by evaluating the residues within the integration path's circle as shown in Fig. 11, which must be zero for an infinite radius. Within the complex plane, there are poles located at $\zeta = \pm z$, zero, and the zeros of Bessel functions. These Bessel functions' zeros are present in both positive and negative directions along the real axis. The zero at $\zeta = 0$ in the denominators of Eq. (B3) is a third-order pole in Q_1, while it is a first-order pole in Q_0.

Consequently, we derive the identity equations for the respective integrals as presented below:

$$Q_0 = \frac{1}{z^2}\left(\frac{1}{J_0^2(z)} - 1\right) + \sum_{k=1}^{\infty}\left[\frac{(-6J_1[j_{0k}] + j_{0k}J_2[j_{0k}])}{(j_{0k}^2 - z^2)^2 J_1^3[j_{0k}]}\right.$$
$$\left. - \frac{z^2(-2J_1[j_{0k}] + j_{0k}J_2[j_{0k}])}{(j_{0k}^2 - z^2)^2 j_{0k}^2 J_1^3[j_{0k}]}\right] = 0, \quad \text{(B4)}$$

and

$$Q_1 = \frac{1}{z^2 J_1^2(z)} - \frac{(4 + z^2)}{z^4}$$
$$- \sum_{k=1}^{\infty}\left[\frac{8(3J_0[j_{1k}] - J_2[j_{1k}])}{(j_{1k}^2 - z^2)^2(J_0[j_{1k}] - J_2[j_{1k}])^3}\right.$$
$$\left. - \frac{8z^2(J_0[j_{1k}] + J_2[j_{1k}])}{(j_{1k}^3 - j_{1k}z^2)^2(J_0[j_{1k}] - J_2[j_{1k}])^3}\right] = 0. \quad \text{(B5)}$$

These equations are summarized as the formulas for the Bessel functions:

$$\frac{1}{z^2 J_0^2(z)} = \frac{1}{z^2} + \sum_{k=1}^{\infty} \frac{4}{(j_{0k}^2 - z^2)^2 J_1^2[j_{0k}]}, \quad \text{(B6)}$$

and

$$\frac{1}{z^2 J_1^2(z)} = \frac{(4 + z^2)}{z^4} + \sum_{k=1}^{\infty} \frac{4}{(j_{1k}^2 - z^2)^2 J_0^2[j_{1k}]}, \quad \text{(B7)}$$

where we utilize

$$J_2[j_{0k}] = \frac{2}{j_{0k}} J_1[j_{0k}], \quad \text{(B8)}$$

$$J_2[j_{1k}] = -J_0[j_{1k}]. \quad \text{(B9)}$$

Ultimately, we can derive Eqs. (B1) and (B2) by reexpressing Eqs. (B6) and (B7) utilizing the connection between modified Bessel functions and Bessel functions, given as $I_m[z] = e^{-m\pi j/2} J_m[e^{j\pi/2}z]$.

[1] H. Hotchi, High-power proton accelerators for pulsed spallation neutron sources, AAPPS Bull. 31, 23 (2021).

[2] K. Yamamoto *et al.*, Design and actual performance of J-PARC 3 GeV rapid cycling synchrotron for high-intensity operation, J. Nucl. Sci. Technol. 59, 1174 (2022).

[3] *Handbook of Accelerator Physics and Engineering, 2nd edition*, edited by A. W. Chao, K. H. Mess, M. Tigner, H. Weise, and F. Zimmermann (World Scientific Pub Co Inc., Singapore, 2013).

[4] H. Wiedemann, *Particle Accelerator Physics* (Springer-Verlag, Berlin, Heidelberg, 1998), 2nd ed.

[5] H. Wiedemann, *Particle Accelerator Physics* (Springer, New York, 2015), 4th ed.

[6] K. Y. Ng, Fermilab Technical Memos Report No. FERMI-LAB-TM-2152, 2001.

[7] B. Zötter, Betatron frequency shifts due to image and self fields, in *Proceedings of CAS—CERN Accelerator School: General Accelerator Physics*, edited by P. J. Bryant and S. Turner (Gif-sur-Yvette, France, 1984), p. 253.

[8] Guignard, Selection of formulae concerning proton storage rings, CERN Report No. CERN-77-10, section VIII.2, 1977.

[9] Y. Shobuda, Y. H. Chin, P. K. Saha, H. Hotchi, H. Harada, Y. Irie, F. Tamura, N. Tani, T. Toyama, Y. Watanabe, and M. Yamamoto, Theoretical elucidation of space-charge effects on the coupled-bunch instability at the 3 GeV rapid cycling synchrotron at the Japan Proton Accelerator Research Complex, Prog. Theor. Exp. Phys. 2017, 013G01 (2017).

[10] P. K. Saha, Y. Shobuda, H. Hotchi, H. Harada, N. Hayashi, M. Kinsho, F. Tamura, N. Tani, M. Yamamoto, Y. Watanabe, Y. H. Chin, and J. A. Holmes, Simulation, measurement, and mitigation of beam instability caused by the kicker impedance in the 3-GeV rapid cycling synchrotron at the Japan Proton Accelerator Research Complex, Phys. Rev. Accel. Beams 21, 024203 (2018).

[11] L. J. Laslett, On intensity limitations imposed by transverse space-charge effects in circular particle accelerators, BNL Report No. 7534, 1963, p. 325.

[12] B. Zötter, Coherent Q-shift of a relativistic particle beam in a metal vacuum chamber, CERN Report No. CERN-ISR-TH/72-8, 1972.

[13] Y. Shobuda and K. Yokoya, Resistive wall impedance and tune shift for a chamber with a finite thickness, Phys. Rev. E 66, 056501 (2002).

[14] S. Kheifets, Potential of a three-dimensional Gaussian bunch, PETRA Note No. 119 (1. 10.76), 1976, https://bib-pubdb1.desy.de/record/320505/files/Petrakurzmitt.11.10.1976.pdf?version=1.

[15] M. Bassetti and G. Erskine, Closed expression for the electrical field of a two-dimensional Gaussian charge, CERN Report No. CERN ISR TH/80-06, 1980, https://cds.cern.ch/record/122227/files/198005132.pdf.

[16] For example and S. Machida, The Simpsons program 6-D phase space tracking with acceleration computational accelerator physics, AIP Conf. Proc. 297, 459 (1993).

[17] E. D. Courant and H. S. Snyder, Theory of the alternating-gradient synchrotron, Ann. Phys. (N.Y.) 3, 1 (1958).

[18] R. L. Gluckstern, J. van Zeijts, and B. Zötter, Coupling impedance of beam pipes of general cross section, Phys. Rev. E 47, 656 (1993).

[19] T. Imamura, *Butsuri to Green Kansu* (Iwanami, Tokyo, 1978), Chap. 5, pp. 75–108.

[20] M. Abramowitz and I. Stegun, *Handbook of Mathematical Functions-With Formulas, Graphs, and Mathematical Tables* (Dover, New York, 1974).

[21] Y. Shobuda and Y. H. Chin, Rigorous formulation of space-charge wake function and impedance by solving the three-dimensional Poisson equation, Sci. Rep. 8, 12805 (2018).

[22] G. N. Watson, *A Treatise on the Theory of Bessel Functions (Cambridge Mathematical Library)* (Cambridge University Press, Cambridge, England, 1995), 2nd ed.

[23] H. Hochstadt, *The Functions of Mathematical Physics (Pure & Applied Mathematics S.)* (John Wiley & Sons Inc., New York, 1971).

[24] L. J. Slater, *Generalized Hypergeometric Functions* (Cambridge University Press, Cambridge, England, 1966).

[25] High-intensity proton accelerator project team, accelerator technical design report for high-intensity proton accelerator facility project, JAEA Report No. JAERI-Tech 2003-044 (2003), p. 127, 10.11484/jaeri-tech-2003-044.

[26] K. Yokoya, Coordinate systems (2002).

[27] H. Prinz, *Hochspannungsfelder* (München, Oldenbourg, 1969).

[28] Y. Shobuda, Y. H. Chin, and K. Takata, Coupling impedances of a gap in vacuum chamber, Phys. Rev. ST Accel. Beams 10, 044403 (2007).